



3 1293 00876 4783

This is to certify that the

dissertation entitled

SUBMERSED MACROPHYTE-EPIPHYTIC PERIPHYTON

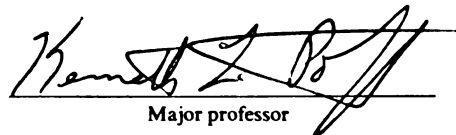
COMMUNITY HYDRODYNAMICS

presented by .

RICHARD FREDERICK LOSEE

has been accepted towards fulfillment
of the requirements for

Ph. D. degree in BOTANY



Major professor

Date 10-14-91

**LIBRARY
Michigan State
University**

PLACE IN RETURN BOX to remove this checkout from your record.
TO AVOID FINES return on or before date due.

DATE DUE	DATE DUE	DATE DUE
01/01/01	_____	_____
_____	_____	_____
_____	_____	_____
_____	_____	_____
_____	_____	_____
_____	_____	_____
_____	_____	_____

MSU is An Affirmative Action/Equal Opportunity Institution

c:\crl\data\due.pm3-p.1

SUBMERSED MACROPHYTE-EPIPHYTIC PERIPHYTON
COMMUNITY HYDRODYNAMICS

By

Richard Frederick Losee

A DISSERTATION

Submitted to
Michigan State University
in partial fulfillment of the requirements
for the degree of

DOCTOR OF PHILOSOPHY

Department of Botany and Plant Pathology

1991

ABSTRACT

SUBMERSED MACROPHYTE-EPIPHYTIC PERIPHYTON COMMUNITY HYDRODYNAMICS

By

Richard Frederick Losee

The transport of dissolved substances across the water column/submersed macrophyte-epiphytic periphyton (M-EP) interface is via molecular diffusion. The rate of this diffusion is a function of the concentration gradient, which is a function of M-EP metabolic activity and the water column concentration. Diffusive flux is also a function of microscale hydrodynamics, which affect the diffusive path length across the M-EP interface. These microscale hydrodynamics are a function of flow rate, M-EP size and shape, and water viscosity.

I measured the magnitude and range of water flow rates within the littoral zones of two lakes of differing morphometry. Measurements within and adjacent to plant beds were made at different depths and among different dominant submersed macrophyte species under different environmental conditions. The mean within bed flow rate was 0.07 cm s^{-1} and individual experiment means ranged from 0.03 cm s^{-1} to 0.46 cm s^{-1} . Flows external to the plant beds were dissipated within the bed in $< 10\text{--}15 \text{ cm}$ from the outer plant-bed boundary even under severe external flow-rate conditions (flow rate $\approx 30 \text{ cm s}^{-1}$). There was very little variability in within-bed flow rates, and factors, such as bed depth and dominant species, had little affect on within-bed flow rate variance.

Microscale flow rate patterns were measured for the M-EP complex under a variety of flow rates, leaf orientations, and water temperatures utilizing video and time-lapse photography. Flow instability or separation associated with submersed macrophyte surfaces was only found at very high flow rates, or localized on the surface of the broad-leaved *P. praelongus* at moderate to fast within-bed flow rates.

Boundary layer thicknesses (δ) measured in this study were much larger ($10^3 \mu\text{m}$) than previously realized. Orientation and presence or

absence of epiphytic periphyton were important in determining δ . An increase in non-filamentous periphyton (i.e., increase in the dimension of projections from the M-EP surface perpendicular to bulk flow direction) decreased δ . Boundary layer thickness also decreased as the angle of M-EP orientation approached 90° to the direction of bulk flow, and δ decreased with increasing water temperature.

These results support the hypothesized mutualism of submersed macrophytes and their epiphytic periphyton.

ACKNOWLEDGMENTS

Many people have provided support of one sort or another during the course of this project. None more than Dr. R.G. Wetzel, whose insights, substantive support, and encouragement made completion of this work possible. I also thank my committee members, Drs. M.J. Klug, K.L. Poff, G.P. Robertson, A.J. Tessier and R.G. Wetzel, for their counsel and critical evaluation of this work. I wish to especially thank Dr. K.L. Poff, who provided invaluable encouragement at critical times, and Mary Losee, who has always been there.

The insights and assistance of all my colleagues at the W.K. Kellogg Biological Station were most helpful, especially those of Drs. R.G. Carlton, W.D. Taylor, J.L. Schuette, R.E. Moeller, M. Coveney, and J.M. Burkholder. Early in the development of this project discussions with Dr. H.H. Riber were central in shaping my perceptions of the subject. T. Davis was of great assistance in the redesign and trouble shooting of the of the flowmeter circuitry. I thank G.P. Robertson for introducing me to Geostatistics which was the tool necessary to solve critical problems. The shepherding of J. Gorentz, W. Mahoney, and S. Ozminski through the mire of large dataset computations was indispensable. Dr. I. Mao provided guidance with the statistical analysis of the "messy" *in situ* flow rate data. C. Hammarskjold's dedication to locating and obtaining obscure and non-ecological references was invaluable. The support of the KBS staff was the lubrication, and more, that made this work possible, in particular, N. Consolatti and S. Marsh.

The research was supported by a grant to R.G. Wetzel by the U.S. Department of Energy (DE-FG02-87ER60515, COO-1599-303), a Michigan State University Graduate Fellowship, and M.H. Losee.

TABLE OF CONTENTS

	Page
LIST OF TABLES	vi
LIST OF FIGURES	vii
INTRODUCTION	1
CHAPTER 1: LITTORAL FLOW RATES IN AND AROUND SUBMERSED MACROPHYTE COMMUNITIES	5
Introduction	5
Materials and Methods	7
Field Measurements	7
Results	11
Discussion	17
CHAPTER 2: SUBMERSED MACROPHYTE-EPIPHYTIC PERIPHYTON MICROSCALE FLOW PATTERNS	27
Introduction	27
Materials and Methods	28
Results	34
Flow Stability	34
Microscale Flow Patterns and Rates	37
Discussion	46
Flow Stability	46
Microscale Flow Patterns and Rates	49
SUMMARY:	55
APPENDIX:	59
Five-channel, Warm-bead Thermistor Flowmeter	59
Circuit	59
Probe	61
Adjusting Temperature Range and Zero	61
Calibration	62
LIST OF REFERENCES:	66

LIST OF TABLES

Table		Page
1	Table 1. Compilation of mean and standard deviation of littoral flow rates (cm s^{-1}) for the 9 measurement locations (see Figure 2). Location mean flow rates with equal superscripts were not significantly different ($\alpha=0.05$) for multiple comparisons within experiments. Mh = <u>Myriophyllum heterophyllum</u> Michx., Ss = <u>Scirpus subterminalis</u> Torr., and Pi = <u>Potamogeton illinoensis</u> Morong. L = leeward, W = windward. Wind speed (m s^{-1}).	13
2	Multifactor covariate analysis of the 60-second interval subset of the Lawrence Lake littoral flow rate data set. $P<0.001$ ***	14
3	Multiple comparisons of mean littoral flow rates (cm s^{-1}) for locations measured simultaneously at 2- and 4-m depths, Experiments 12 and 13, respectively. Locations with equal superscripts were not significantly different, $\alpha=0.05$	16
4	Multiple comparisons of mean littoral flow rates (cm s^{-1}) for corresponding locations across depths and experiments. Locations with equal superscripts were not significantly different, $\alpha=0.05$	17
5	Multiple comparisons of mean littoral flow rates (cm s^{-1}) for locations measured simultaneously in <u>S. subterminalis</u> and <u>P. illinoensis</u> dominated beds. Locations with equal superscripts were not significantly different, $\alpha=0.05$	17
6	Multifactor covariate analysis of within-bed location flow rates using a 60-second interval subset of the Lawrence Lake data set. $P<0.001$ ***	20
7	Summary of the <u>S. subterminalis</u> microscale flow pattern experiments. δ is the average and δ_{calc} the predicted distance Z from the surface where du/dz approached 0 for the region perpendicular to flow. U is the free stream velocity and l is the average of the length and width dimensions for the cross section.	45

LIST OF FIGURES

Figure		Page
1	Conceptual illustration of laminar flow boundary layer (LBL) development.	4
2	Probe locations within and around the submersed macrophyte beds: L1- 15-20 cm above the canopy, L2- 10-15 cm below the upper canopy limit, L3- 25-30 cm below the upper canopy limit, L4- 40-45 cm below the upper canopy limit and 50 cm inside the lakeward edge of the bed, L5- 10-15 cm above the sediment, L6- 40 cm inside the lakeward edge, L7- 20 cm inside the lakeward edge, L8- 10 cm inside the lakeward edge of the bed, and L9- 15-25 cm outside the lakeward edge of the bed.	9
3	Example of a typical semivariogram: Experiment 9, position L4 (40-45 cm below the upper canopy and 50 cm inside the lakeward edge of the 2-m <u>S. subterminalis</u> bed). LAG(h) in seconds. . . .	12
4	Box plot of flow rate measurements for locations L1 - L9. The box divides are at the 1 st , 2 nd , and 3 rd quartiles, and the bottom and top bounds are the 5 th and 95 th flow rate percentiles, respectively. The solid dots are the flow rate measurements outside this range. Note the break in the vertical scales. The inset is the composite of within- and outside-bed flow rate measurements.	15
5	Theoretical momentum boundary layer development over a flat surface for the minimum mean, mean for the study, and maximum mean flow rates. δ = boundary layer thickness, l = distance from the leading edge.	21
6	Typical flow rate versus time plot for Experiment 8, 0.5 second measurement interval (see Figure 2 for probe locations).	25
7	Flume and camera setup for video- and time-lapse photography of flow around submersed macrophyte leaves. See text for explanation.	29
8	Semivariograms of flow rate in the plane parallel to flow for Experiments 1 through 6.	33
9	Time-lapse photograph of flow pathlines around a <u>P. praelongus</u> leaf. Flow is from right to left, $\approx 0.42 \text{ cm s}^{-1}$, 200 flashes min^{-1} . Upper panel viewed in longitudinal cross section. Note the arching pathline downstream of the leaf tip. Lower panel viewed in lateral cross section.	36

Figure		Page
10	Experiment 2 isopleth of estimated flow rate (upper panel) or standard deviation (lower panel) in the plane parallel to the direction of flow around a <u>S. subterminalis</u> leaf viewed in lateral cross section. The solid lines perpendicular to flow in the upper panel are the estimated δ . Flow is from right to left, rate in cm s^{-1} , epiphytic periphyton present, and water temperature 23°C	38
11	Experiment 5 isopleth of estimated flow rate (upper panel) or standard deviation (lower panel) in the plane parallel to the direction of flow around a <u>S. subterminalis</u> leaf viewed in lateral cross section. The solid lines perpendicular to flow in the upper panel are the estimated δ . Flow is from right to left, rate in cm s^{-1} , epiphytic periphyton present, and water temperature 23°C	39
12	Experiment 1 isopleth of estimated flow rate (upper panel) or standard deviation (lower panel) in the plane parallel to the direction of flow around a <u>S. subterminalis</u> leaf viewed in lateral cross section. The solid lines perpendicular to flow in the upper panel are the estimated δ . Flow is from right to left, rate in cm s^{-1} , epiphytic periphyton present, and water temperature 6°C	40
13	Experiment 3 isopleth of estimated flow rate (upper panel) or standard deviation (lower panel) in the plane parallel to the direction of flow around a <u>S. subterminalis</u> leaf viewed in lateral cross section. The solid lines perpendicular to flow in the upper panel are the estimated δ . Flow is from right to left, rate in cm s^{-1} , epiphytic periphyton absent, and water temperature 23°C	41
14	Experiment 4 isopleth of estimated flow rate (upper panel) or standard deviation (lower panel) in the plane parallel to the direction of flow around a <u>S. subterminalis</u> leaf viewed in lateral cross section. The solid lines perpendicular to flow in the upper panel are the estimated δ . Flow is from right to left, rate in cm s^{-1} , epiphytic periphyton absent, and water temperature 7°C	42
15	Experiment 6 isopleth of estimated flow rate (upper panel) or standard deviation (lower panel) in the plane parallel to the direction of flow around a <u>S. subterminalis</u> leaf viewed in lateral cross section. The solid lines perpendicular to flow in the upper panel are the estimated δ . Flow is from right to left, rate in cm s^{-1} , epiphytic periphyton absent, and water temperature 5°C	43
16	Conceptual illustration of right to left flow streamlines around small submersed plant leaf with and without epiphytic periphyton, right and left panels respectively.	51

Figure		Page
17	Flowmeter circuit schematic.	60
18	Measured calibration curve and predicted flow rate versus flowmeter millivolts output for each probe and paired circuit.	64

INTRODUCTION

Numerous investigators have observed for submersed aquatic plants that photosynthesis, respiration, and mineral uptake rates increase with increasing flow rate (Barth 1957, Whitford and Schumacher 1961, Schumacher and Whitford 1965, Westlake 1967, Madsen and Søndergaard 1983, Wheeler 1980). Other authors have also recognized the importance, among submersed plants, of boundary layer diffusive resistance to the uptake of nutrients, particularly inorganic carbon (cf. Munk and Riley 1952, Gavis 1976, Raven 1970, Smith and Walker 1980). However, these authors based their conclusions on results from highly artificial experimental protocol or theory, and, as a result, have underestimated the importance of diffusive resistance. Diffusive transport of dissolved substances and gases across the water column/macrophyte-epiphytic periphyton (M-EP) interface govern biological and chemical activity within the M-EP complex under commonly occurring conditions. In addition, the M-EP community role in regulating the dissolved nutrients, organic matter, and anthropogenic compounds of the aquatic ecosystem is mediated by transport across the interface.

On the premise of Fick's first law of diffusion ($J = -D(dc/dz)$ where J is the diffusive flux of a gas or dissolved substance across the interface, D is the diffusion coefficient, and dC/dz is the concentration gradient (Crank 1975)), biological activity is affected by resistance to transport when there is a significant concentration gradient of assimilates or waste products across the water column/M-EP interface. For example, diffusive resistance to inorganic carbon transport across the water column/M-EP complex interface limits photosynthesis by limiting the supply of inorganic carbon, and by maintaining an elevated level of photosynthetically produced O_2 within

the complex. The elevated O_2 and depleted CO_2 compete for the photosynthetic enzyme ribulose-bisphosphate carboxylase oxygenase.

Diffusive flux (J) is inversely proportional to the diffusive path length. The diffusive path length demarcates the concentration or diffusion boundary layer (DBL) thickness, and is the distance (z) from the M-EP surface where dC/dz approaches 0. Where the flow over submersed plant surfaces is laminar, the transport of dissolved substances across the water column/M-EP interface is via molecular diffusion. Therefore, because molecular diffusion is such a slow process, the diffusive path length is a critical parameter determining the flux rate.

The occurrence of turbulent flow associated with the M-EP complex may be predicted from the ratio of inertial to viscous forces known as the Reynolds number (Re): $Re = \rho l U / \mu = l U / \nu$ where ρ is density ($kg\ m^{-3}$) of water, l is a characteristic dimension (m) of the object (i.e., diameter, or distance from the leading edge of the leaf), U is free-stream flow rate ($m\ s^{-1}$), μ is dynamic viscosity ($kg\ m^{-1}\ s^{-1}$), and ν is kinematic viscosity ($m^2\ s^{-1}$) (Vogel 1981). Dynamic viscosity is the coefficient which relates the shear stress (force \times area $^{-1}$ time $^{-1}$) to the local velocity gradient or shear rate, and kinematic viscosity is the ratio of dynamic viscosity to density (Vogel 1981). For a smooth, flat surface, the transition from laminar to turbulent flow occurs when the Re exceeds a critical value of about 5×10^5 (Leyton 1975). This does not preclude the possibility of turbulent flow associated with the surface at a lower Re .

Up to this time, methods for measuring flow rates within submersed plant beds have not been very satisfactory, because spatial and temporal resolution is lacking (cf. Madsen and Warncke 1983, Machata-Wenninger and Janauer 1991). Nonetheless, estimates of within submersed macrophyte bed flow rates published by these authors range from 0.3 to 5 $cm\ s^{-1}$. An order-of-magnitude calculation of Re for a submersed macrophyte leaf yields a $Re = 100$, where $l = 0.01\ m$, $U = 0.01\ m\ s^{-1}$, and

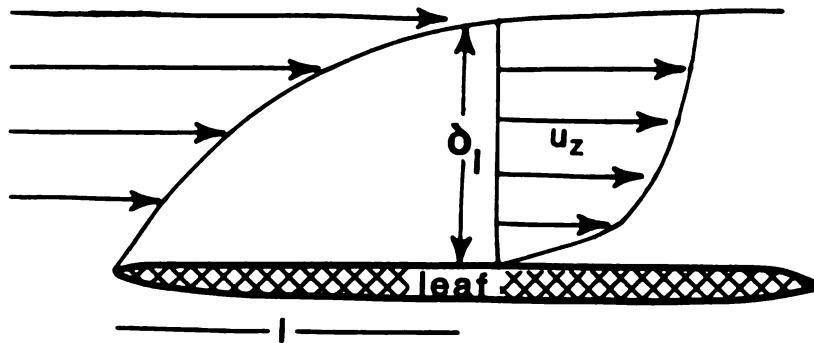
$\nu = 10^{-6} \text{ m}^2 \text{ s}^{-1}$. This Re is small; viscous forces dominate and laminar flow is expected to surround M-EP surfaces (Leyton 1975). Although turbulent eddies occur in the "bulk" phase or free stream region in the littoral water column not directly affected hydrologically by submersed surfaces, these eddies are involved with bulk transport in the littoral water column rather than across the plant surface/water column interface.

The thickness of the laminar flow boundary layer (LBL) surrounding the M-EP complex is variable and dependent on several parameters. LBL thickness (δ) may be estimated by utilizing a functional definition: the boundary layer thickness is the distance (z) normal to the plant surface where flow rate (u_z) is 99% of the free stream rate (Figure 1). Then

$$\delta = 5 l Re_l^{-1/2} \text{ or } \delta = 5 (\nu l / U)^{1/2} \text{ (Leyton 1975).}$$

Using an order-of-magnitude calculation as performed for Re , (δ) was estimated to be one to several millimeters thick (Losee and Wetzel 1988, also see Silvester and Sleigh 1985). The LBL is related to the DBL because turbulence (which, by definition, occurs only outside of the LBL) tends to maintain $dc/dz=0$ at the LBL limit as a result of the greater rate of eddy versus molecular diffusive transport. Hence, diffusive resistance surrounding M-EP surfaces is likely to be substantial in nature and highly dependent on the flow rate as well as viscosity and M-EP size and orientation.

This study consists of two components. The objective of the first component was to characterize littoral flow rate magnitude and duration with respect to location within and around submersed plant beds. Of interest was the relationship among littoral flow rates and submersed plant bed depth, dominant species, wind direction and wind speed. The objective in the second component was to determine the pattern and rates of flow around the submersed M-EP complex for various flow rates, water temperatures, and M-EP complex conditions (i.e., orientation, presence or absence of epiphytic periphyton, and species of macrophyte) with regard to LBL development.



U = free stream velocity

u = laminar flow velocity height z above the surface

δ = boundary layer thickness distance l from the leading edge

$$\delta_l = 5l(Re)^{-1/2} = 5(l\nu/U)^{1/2}$$

Figure 1. Conceptual illustration of laminar flow boundary layer (LBL) development.

CHAPTER 1

LITTORAL FLOW RATES IN AND AROUND SUBMERSED MACROPHYTE COMMUNITIES

INTRODUCTION

A gradient of increasing flow rate occurs perpendicular to the submersed macrophyte-epiphytic periphyton (M-EP) surface. This gradient results from the "no-slip" condition (i.e., the adhesion of a layer of water molecules via intermolecular forces to submersed surfaces) and the viscous nature of water. Since the ratio of inertial to viscous forces (Reynolds number, Re) is small for submersed macrophytes, laminar flow is expected to surround M-EP surfaces. Where the flow over submersed plant surfaces is laminar, the transport of gases and dissolved substances across the water column/M-EP surface interface is via molecular diffusion following Fick's first law: $J = -D(dC/dz)$ where J is the diffusive flux of a dissolved substance across the interface, D is the diffusion coefficient, and dC/dz is the concentration gradient (Crank 1975).

The concentration or diffusion boundary layer (DBL) thickness, z (where dC/dz approaches 0), is a function of microscale hydrodynamics and the dissolved substance supply and demand across the interface. Turbulence outside the laminar flow boundary layer (LBL) (distance z normal to the surface where du/dz approaches 0, u is flow rate) will tend to maintain $dC/dz=0$ as a result of the greater rate of eddy versus diffusive transport. It is in this region, where du/dz approaches 0, that the transition from laminar flow over a plant surface to turbulent littoral zone flow occurs.

From Fick's first law, the concentration gradient is a scaling factor controlling the flux of dissolved substances across the water

column/plant surface interface. As long as a concentration difference exists across the interface, the diffusive path length (equivalent to DBL thickness in this model) is important in affecting the resistance to the transport of dissolved substances across the interface. This relationship indicates that the transport of gases and dissolved substances across the interface is affected by the diffusive resistance of the boundary layer. In a study where LBL thickness was carefully controlled, Riber and Wetzel (1987) found that phosphorus fluxes across the water column/periphyton interface were limited by boundary layer transport. Tracer fluxes were described as a power function of flow rate and by a negative function of distance from the leading edge of the periphyton community. Among submersed plants, the importance of boundary layer diffusive resistance to the uptake of nutrients, particularly inorganic carbon, has been recognized by several authors (cf. Munk and Riley 1952, Gavis 1976, Raven 1970, Smith and Walker 1980).

The thickness of the LBL surrounding submersed plant surfaces is variable and dependent on several parameters. LBL thickness (δ) may be estimated by utilizing a functional definition: the boundary layer thickness is the distance (z) normal to the plant surface where flow rate (u_z) is 99% of the free stream rate. Then

$\delta \approx 5 l Re_l^{-1/2}$ or $\delta \approx 5 (vl/U)^{1/2}$ (Leyton 1975). Estimates of (δ) range from one to several millimeters thick (Losee and Wetzel 1988, also see Silvester and Sleight 1985). Hence, diffusive resistance surrounding M-EP surfaces is likely to be substantial in nature and highly dependent on the flow rate. An example of the effect of flow rate on boundary layer diffusive resistance and its impact on metabolic activity is the increase in submersed plant tissue photosynthetic activity with increased flow rate noted by Barth (1957), Westlake (1967), and Madsen and S ndergaard (1983).

The objectives of this study were to characterize littoral flow rate magnitude and duration with respect to location within and around

submersed plant beds. In addition, I investigated the relationship among littoral flow rates and submersed plant bed depth, dominant species, wind direction and wind speed.

MATERIALS AND METHODS

Littoral flow rates within and around submersed macrophyte beds were measured with a 5-channel warm-bead thermistor flowmeter, modified from Vogel (1981) (Appendix). The principle of operation for the flowmeter is as follows. An electrical current passing through a thermistor bead heated the bead to an equilibrium temperature that is a function of the electrical power applied and the heat dissipation characteristics of the surrounding medium. Cooling by forced convection is a strong function of flow rate. In an isothermal circuit, where the sensing thermistor is maintained at a set temperature above ambient, the electrical power required to maintain the temperature offset is a function of flow rate. A small sensing thermistor, 0.4-mm diameter (Thermometrics, Inc., BR16KA251M, nominal resistance 250 Ohms), was used to improve spatial and temporal resolution by decreasing probe size and thermal inertia. The temperature compensation thermistor was Thermometrics, Inc., Model BR32KB103M, nominal resistance 10K Ohms. Forstner and Rützler (1969) and Riedl and Machan (1972) discuss hot-bead thermistor flow measurement theory. Voltage output from the flowmeter, proportional to flow rate, was measured and stored at various intervals with a Campbell CR21 Micrologger or a Campbell CR10 Datalogger. Measurement intervals chosen were a compromise between the temporal resolution desired for the experiment and the storage capacity of the data logger. Flowmeter calibration (Appendix) was periodically checked before and after a measurement series to guard against electronic drift. When drift occurred, the data were discarded.

Field Measurements

Experiments were conducted in two north temperate lakes: the

smaller, Lawrence Lake, had a mean depth of 5.9 m and a surface area of 4.7 ha (Rich et al. 1971); and the larger, Gull Lake, had a mean depth of 12.4 m and a surface area of 822 ha. (Moss 1972a, b). Flow probes were arrayed vertically and/or horizontally through the plant beds and were clamped to a 1.3-cm diameter aluminum rod. The probes were held away from the rod with laboratory clamps. SCUBA was used to position the probes and carefully thread the cables through the vegetation to prevent interference with measurements. Care was taken to ensure that the sensing thermistor was not in contact with vegetation. The vertical rod was inserted nearly a meter into the sediment, which provided a secure mooring against the flow rates encountered. A horizontal rod was clamped to the vertical rod to accommodate the probes horizontally arrayed through the plant beds toward open water, such that they were oriented perpendicular to the shore and parallel to the water surface. Probe cables were 15 m long to allow the remote stationing of the flowmeter and data logger and to permit down-loading of the data to a portable computer in the field without disturbing the apparatus.

Experiments were conducted in five nearly monospecific plant beds, one each of Myriophyllum heterophyllum Michx. and Potamogeton illinoensis Morong., and three of Scirpus subterminalis Torr. The M. heterophyllum bed (Experiment 1) was located at 3-m depth in Gull Lake. The remaining beds were in Lawrence Lake on the steep littoral slope. The P. illinoensis bed (Experiments 15, 17, 19) was located at 1.5 m depth, and the S. subterminalis beds were located at 1.5-m (Experiment 2), 2.0-m (Experiments 3-10, 12, 14, 16, 18), and 4.0-m (Experiments 11, 13) depths. Over the course of the study measurements were made at nine locations in and around the plant beds. Probe locations are illustrated in Figure 2.

Wind direction and speed were obtained as hourly averages from the W. K. Kellogg Biological Station weather station, located 5 km from Lawrence Lake at Gull Lake. Two classes of wind direction were recognized, windward and leeward.

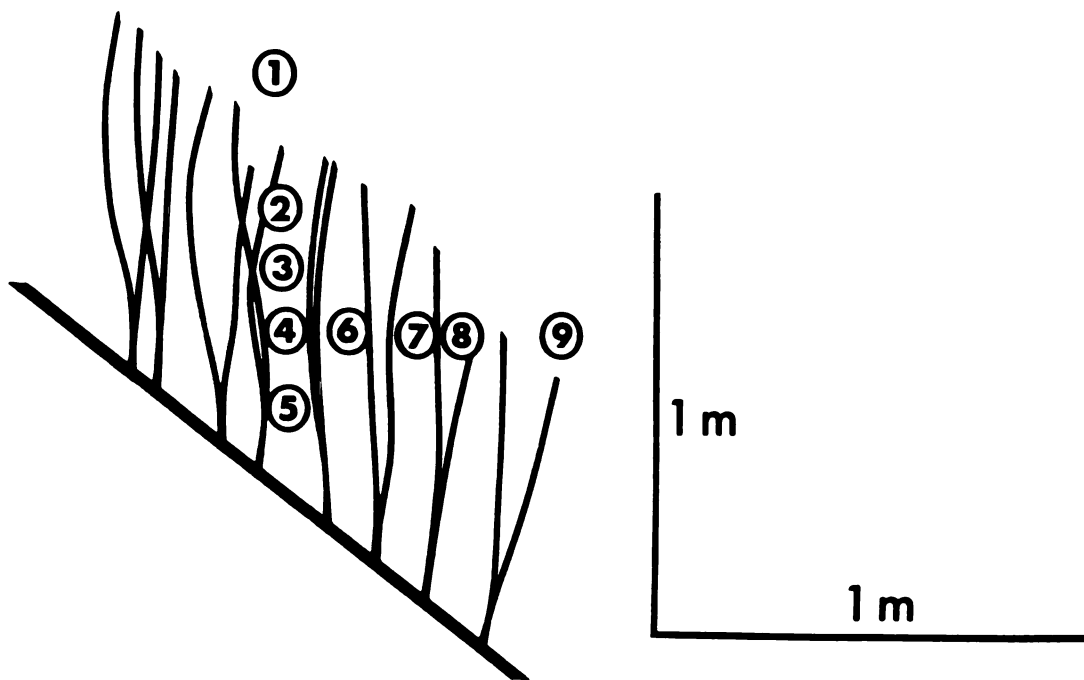


Figure 2. Probe locations within and around the submersed macrophyte beds: L1- 15-20 cm above the canopy, L2- 10-15 cm below the upper canopy limit, L3- 25-30 cm below the upper canopy limit, L4- 40-45 cm below the upper canopy limit and 50 cm inside the lakeward edge of the bed, L5- 10-15 cm above the sediment, L6- 40 cm inside the lakeward edge, L7- 20 cm inside the lakeward edge, L8- 10 cm inside the lakeward edge of the bed, and L9- 15-25 cm outside the lakeward edge of the bed.

Plant surface area per sediment area was determined by sampling 20 cm x 30 cm plots at the flow measurement sites. All above-ground vegetation was removed for plants rooted within the plot. Total plant surface area for each plot was measured with a Licor Area Meter, model 3100.

The relative importance of five factors in determining littoral flow rates within and around submersed macrophyte beds was investigated by performing a multifactor covariate analysis (SAS Institute 1988) on the Lawrence Lake data set. The model described flow rates as a function of plant bed depth, dominant species, location within and around the plant bed, and wind direction and speed: $\text{Flow rate} = \mu + \text{Depth} + \text{Species} + \text{Location} + \text{Wind direction} + b(\text{Wind speed}) + \text{error}$. Rate observations were averaged over various time intervals ranging from 0.5 - 120 seconds. A priori, some autocorrelation (correlation resulting from proximity of samples in time) was expected in the data, which would violate the statistical assumption of independence of each observation. For this reason I adopted the following strategy: the degree of autocorrelation of the data was determined, and the data set subsampled at a time interval where the autocorrelation was insignificant. The degree of autocorrelation was determined with the semi-variance statistic ($\gamma(h)$) of the geostatistical procedure described by Webster (1985) and Robertson (1987), and with the computer program provided by Robertson (1987). The semi-variogram is a function which describes the change in semi-variance statistic ($\gamma(h)$) with an increase in time interval:

$$\gamma(h) = \frac{1}{2N(h)} \sum_{i=1}^{N(h)} [z(x_i) - z(x_{i+h})]^2$$

where $z(x_i)$ is the flow rate at time x , $z(x_{i+h})$ is the value at time x_{i+h} , and $N(h)$ is the total number of sample point contrasts for the time interval h . The resulting plot of $\gamma(h)$ versus time interval class is the semivariogram. Autocorrelation becomes insignificant where the semi-variogram flattens. This time interval was often less than 30 seconds and certainly less than 60 seconds (Figure 3) for the littoral

flow data of this study. Therefore, when data were collected at intervals of less than 60 seconds, statistics were calculated on subsets of the data created by sampling the original data at 60-second intervals.

Tukey's multiple comparisons procedure (SAS Institute 1988) was used to investigate, in greater detail, the main effects determining littoral flow rates: depth, dominant species, and location within and around a submersed plant bed. Locations were compared within each experiment where observations for the various locations were made simultaneously (Table 1). In this way, the remaining factors were either held constant or were equal across locations for each observation. Specific experiments were designed to investigate the importance of the main effects depth of plant bed (Experiments 9, 10, 11, 12 and 13) and dominant species (Experiments 14, 15, 16, 17, 18 and 19).

RESULTS

Minimum, maximum, and mean littoral flow rates, compiled by experiment for the nine measurement locations within and around submersed plant beds, were remarkably similar (Table 1). Littoral flow rates were measured over a wide range of conditions varying from mean outside-bed flow rates of 0.09 cm s^{-1} (Experiment 11) to $\approx 30 \text{ cm s}^{-1}$ (Experiment 4). The total submersed macrophyte surface area ranged from $4.14 \text{ m}^2 \text{ m}^{-2}$ of lake sediment for the 1.5-m depth *P. illinoensis* bed, to $15 \text{ m}^2 \text{ m}^{-2}$ of lake sediment for the 2-m depth *S. subterminalis* bed. The mean within-bed flow rates ranged from 0.03 cm s^{-1} to only 0.46 cm s^{-1} . Over the course of 70 within-bed flow measuring hours, the 95th percentile of measured flow rates was approximately 0.15 cm s^{-1} , and the second quartile was 0.08 cm s^{-1} . In contrast, over the course of 53 outside-bed flow measuring hours, the 95th percentile of measured flow rates was approximately 1.5 cm s^{-1} , and the second quartile was 0.5 cm s^{-1} (Figure 4). The relatively high mean littoral flow rates

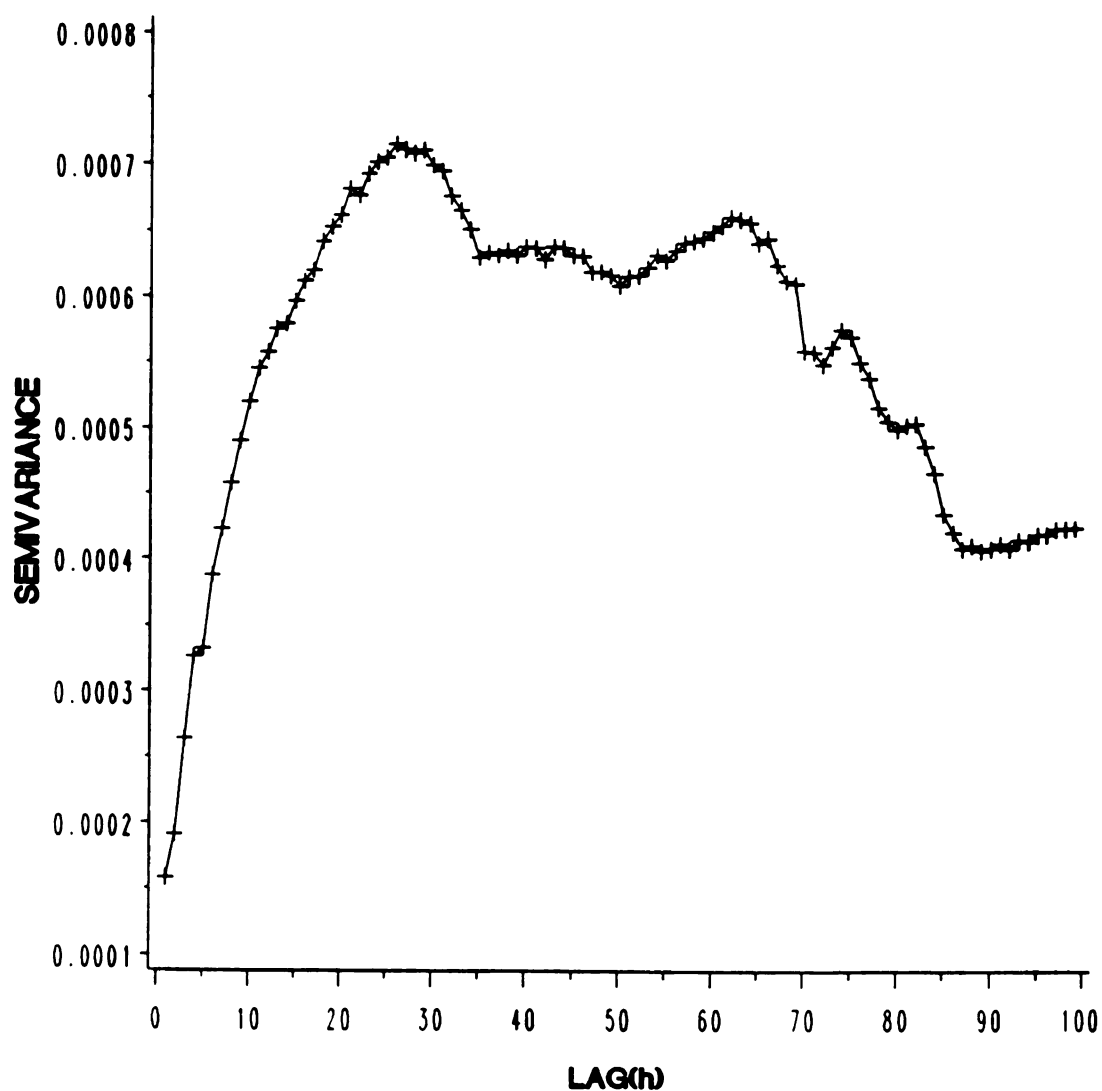


Figure 3. Example of a typical semivariogram: Experiment 9, position L4 (40-45 cm below the upper canopy and 50 cm inside the lakeward edge of the 2-m S. subterminalis bed). LAG(h) in seconds.

Table 1. Compilation of mean and standard deviation of littoral flow rates (cm s^{-1}) for the 9 measurement locations (see Figure 2). Location mean flow rates with equal superscripts were not significantly different ($\alpha=0.05$) for multiple comparisons within experiments. Mh = *Myriophyllum heterophyllum* Michx., Ss = *Scirpus subterminalis* Torr., and Pi = *Potamogeton illinoensis* Morong. L = leeward, W = windward. Wind speed (m s^{-1}).

Expt #	Species	Depth (m)	Wind direction	Wind speed	L1		L2		L3		L4		L5		L6		L7		L8		L9	
					Mean	SD	Mean	SD	Mean	SD	Mean	SD	Mean	SD	Mean	SD	Mean	SD	Mean	SD	Mean	SD
1	Mh	3.0	L	3.5	2.30						0.43						0.19				0.65	
2	Ss	1.5	W	4.0							^B 0.35	0.03					^B 0.44	0.16			^A 5.56	3.01
3	Ss	2.0	W	4.3	^A 3.65	1.48	^B 0.28	0.03					^B 0.46	0.12								
4	Ss	2.0	W	4.6	^A 2.30	-	^B 0.43	0.12					^C 0.34	0.06								
5	Ss	2.0	W	3.0	^A 1.00	0.42	^C 0.07	0.01					^C 0.08	0.02			^C 0.05	0.01			^B 0.40	0.44
6	Ss	2.0	W	3.0	^A 0.19	0.14	^C 0.05	0.00	^C 0.05	0.01	^B 0.12	0.04	^C 0.07	0.00								
7	Ss	2.0	L	4.8	^A 0.21	0.11	^C 0.05	0.03	^C 0.08	0.01	^C 0.05	0.00	^B 0.14	0.01								
8	Ss	2.0	L	4.8	^A 0.25	0.10	^C 0.04	0.01	^C 0.07	0.01	^C 0.05	0.01	^B 0.14	0.01								
9	Ss	2.0	L	2.9							^B 0.11	0.01			^B 0.06	0.01	^B 0.10	0.02	^B 0.06	0.04	^A 0.37	0.42
10	Ss	2.0	L	3.0							^B 0.09	0.01			^B 0.05	0.02	^B 0.08	0.02	^B 0.12	0.23	^A 1.22	0.79
11	Ss	4.0	L	3.0							^A 0.11	0.01			^D 0.04	0.01	^C 0.06	0.00	^D 0.05	0.01	^B 0.09	0.03
12	Ss	2.0	W	2.2							^B 0.08	0.01							^C 0.03	0.01	^A 0.26	0.20
13	Ss	4.0	W	2.2															^B 0.04	0.00	^A 0.36	0.29
14	Ss	2.0	W	2.5															^B 0.03	0.00	^A 0.08	0.04
15	Pi	1.5	W	2.5											^B 0.09	0.02			^B 0.05	0.01	^A 0.20	0.17
16	Ss	2.0	W	2.5															^B 0.03	0.00	^A 0.14	0.14
17	Pi	1.5	W	2.5											^B 0.08	0.01			^B 0.04	0.01	^A 0.51	0.27
18	Ss	2.0	W	2.9															^B 0.03	0.00	^A 0.25	0.27
19	Pi	1.5	W	2.9											^B 0.01	0.07					^A 1.23	1.48

(Experiments 1-4) were found when the mixed layer was deep or the lake was isothermal.

Multifactor covariate analysis of the Lawrence Lake data, with main effects of submersed plant bed depth, dominant species, within and around bed location, and wind direction, and wind speed as covariate, revealed that all main effects and the covariate were significant (Table 2). In a more detailed analysis, multiple comparisons of location mean flow rates were performed on experiments designed to investigate specific main effects.

Table 2. Multifactor covariate analysis of the 60-second interval subset of the Lawrence Lake littoral flow rate data set. $P < 0.001$ ***

Sources of Variation	df	F value
Depth	2	253.97 ***
Species	1	208.56 ***
Location	8	273.47 ***
Wind direction	1	13.45 ***
Wind speed	1	553.13 ***

Multiple comparisons of location flow rates were performed within each experiment (Table 1). Within an experiment, location means with the same superscript were not significantly different. In all cases except one (Experiment 11), outside-bed flow rates were significantly greater than within-bed rates. In 7 of 13 experiments with multiple within-bed measurement locations, mean flow rates for these locations were not significantly different.

Five experiments (9, 10, 11, 12, 13) were designed to investigate the importance of water depth of macrophytic community on littoral flow rates within and around *S. subterminalis* beds. A multifactor covariate analysis of these experiments showed depth was only slightly significant

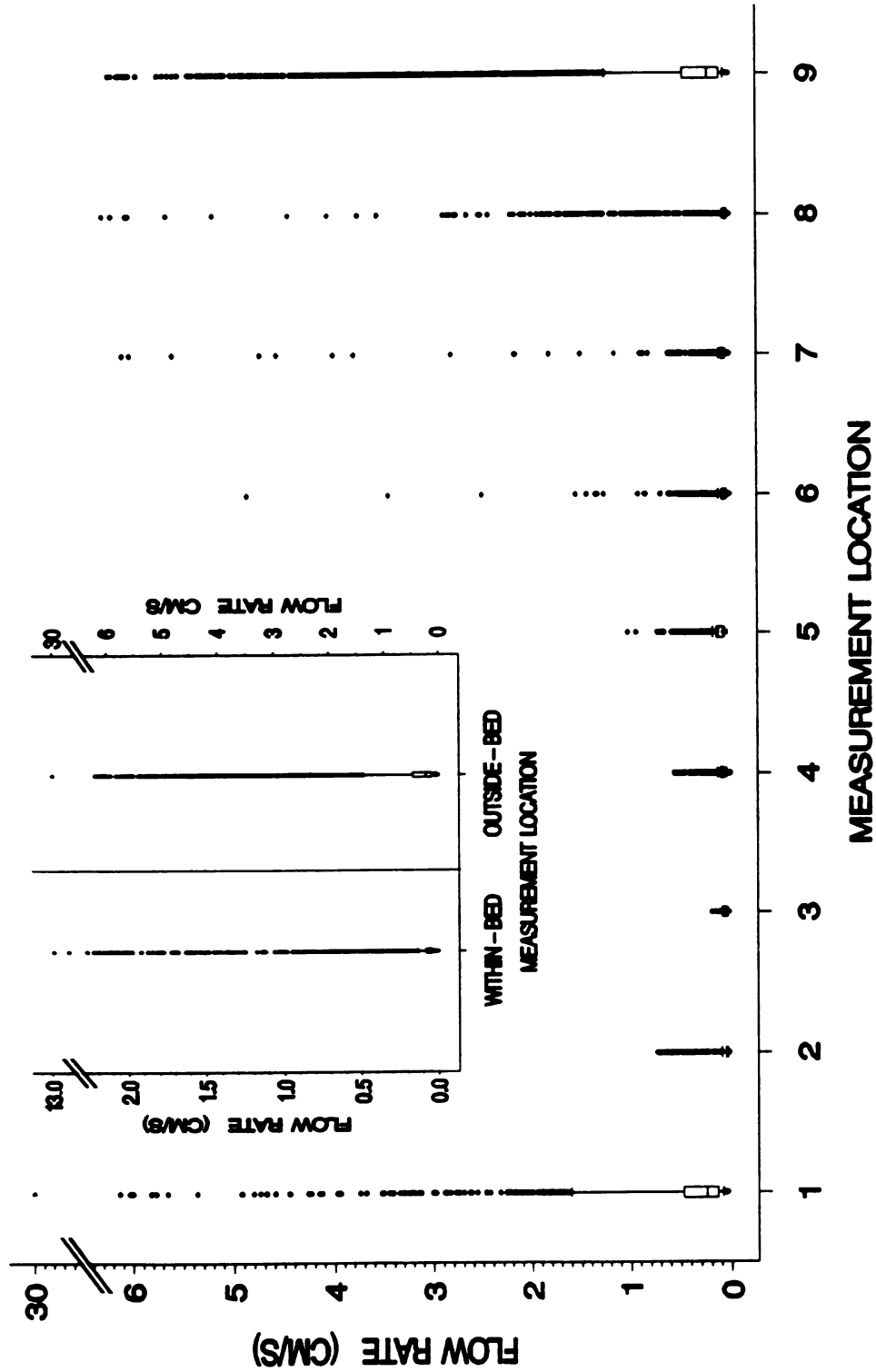


Table 3. Multiple comparisons of mean littoral flow rates (cm s^{-1}) for locations measured simultaneously at 2- and 4-m depths, Experiments 12 and 13, respectively. Locations with equal superscripts were not significantly different, $\alpha=0.05$.

Expt. #	L4	L8	L9
12	0.08 ^c	0.03 ^d	0.26 ^b
13		0.04 ^{cd}	0.36 ^a

($P < 0.1$). Experiments 12 (2-m depth) and 13 (4-m depth) were conducted simultaneously and permitted multiple comparisons across depths for the five locations in the two plant beds (Table 3). Outside-bed flow rates were significantly different, but within-bed rates for the corresponding location (10 cm inside the open water edge (L8)), in the 2- and 4-m depth beds were not significantly different. Multiple comparisons were performed for corresponding locations across Experiments 9, 10 (2-m depth) and 11 (4-m depth) (Table 4). Over the 3.5 hours of the three experiments, the mean hourly wind speed increased from 2.9 to 3.5 m s^{-1} . In no case were corresponding within-bed locations in the two beds significantly different, even though outside the lakeward edge of the bed flow rates were significantly different for all three experiments.

Three pairs of experiments (14 & 15, 16 & 17, 18 & 19) were designed to investigate the importance of dominant plant bed species on littoral flow rates within and around the S. subterminalis and P. illinoensis beds. Multifactor covariate analysis of these six experiments showed dominant species was significant ($P < 0.001$). In these experiments, wind direction was not significant. Paired experiments were conducted simultaneously, which permitted multiple comparisons within paired experiments (Table 5). Once again, within-bed location flow rates were not significantly different for the two beds, even though flow rates outside the lakeward edge of the two beds were always significantly different.

Table 4. Multiple comparisons of mean littoral flow rates (cm s^{-1}) for corresponding locations across depths and experiments. Locations with equal superscripts were not significantly different, $\alpha=0.05$.

Expt. #	L4	L6	L7	L8	L9
9	0.11 ^A	0.06 ^A	0.10 ^A	0.06 ^A	0.37 ^B
10	0.09 ^A	0.05 ^A	0.08 ^A	0.12 ^A	1.22 ^A
11	0.11 ^A	0.04 ^A	0.06 ^A	0.05 ^A	0.09 ^C
Experiments 9, 10 and 11 were run consecutively with locations identical in experiments 9 and 10 (2-m <i>S. subterminalis</i> bed), and experiment 11 (4-m <i>S. subterminalis</i> bed) measurements were made at locations corresponding with the 2-m depth experiments'.					

Table 5. Multiple comparisons of mean littoral flow rates (cm s^{-1}) for locations, measured simultaneously in *S. subterminalis* and *P. illinoensis* dominated beds. Locations with equal superscripts were not significantly different, $\alpha=0.05$.

Expt. #	<i>S. subterminalis</i>		<i>P. illinoensis</i>		
	L8	L9	L6	L8	L9
14 & 15	0.03 ^B	0.08 ^B	0.10 ^B	0.05 ^B	0.20 ^A
16 & 17	0.03 ^C	0.14 ^B	0.08 ^{BC}	0.04 ^{BC}	0.51 ^A
18 & 19	0.03 ^C	0.25 ^B	0.10 ^C	-	1.23 ^A

DISCUSSION

This study characterized the magnitude and range of littoral flow rates, particularly within plant beds at different depths and among different dominant submersed plant species. The outstanding feature of littoral flow was the slow within-bed flow rates, regardless of external flow rates (Table 1, Figure 4). The mean within-bed flow rate for the study was 0.07 cm s^{-1} , with a minimum mean within-bed flow rate of 0.03 cm s^{-1} , and a maximum mean within-bed flow rate of only 0.46 cm s^{-1} .

Flow rates were $< 0.15 \text{ cm s}^{-1}$ for 97% of the within-bed flow measuring hours. These rates contrast with outside-bed flow rates $>0.25 \text{ cm s}^{-1}$ 74% and $>1 \text{ cm s}^{-1}$ 26% of the time. During only one experiment (Experiment 9), were very rapid within-bed maximum flow rates recorded ($>10 \text{ cm s}^{-1}$), probably the result of fish briefly swimming near the sensors. These rapid flow rates were probably of little significance in terms of transport across the water column/plant surface interface because they occurred so infrequently. Flow rates were relatively slow even within the Gull Lake Myriophyllum heterophyllum winter-bed (Experiment 1, Table 1) where the plants were slight and sparse ($\approx 80 \text{ plants m}^{-2}$) and the lake surface area was much larger and more exposed than Lawrence Lake.

All factors of the model describing littoral flow rates were highly significant in the multifactor covariate analysis of the Lawrence Lake data set. Main effects (plant bed depth, dominant species, measurement location, wind direction, and wind speed) but not interaction terms were included in the analysis. The study was designed as an exploratory investigation to determine the range of within-bed flow rates and relative importance of these factors.

Multiple comparisons of mean flow rates within experiments showed that outside-bed flow rates were significantly greater than within-bed rates for all cases but one. This difference between within- and outside-bed flow rates accounted for much of the location factor variance. There was some variability in within-bed flow rates, with within-bed rates significantly different in 6 of 13 experiments which had multiple measurement locations within a bed. The higher within-bed flow rates occurred predominately near the bottom of the S. subterminalis bed (in the L4 and L5 positions, Figure 2). Scirpus subterminalis has opposite leaves arising from a sheath one to a few cm above the sediment (Burkholder and Wetzel 1989). Therefore, less plant surface density (surface area per volume of water) occurs just above the sediment than occurs higher in a S. subterminalis bed. In general, the

spatial pattern of within-bed flow rates is most likely a function of plant surface density throughout the volume of the bed, as the edge effect has been dissipated in less than 10-15 cm for the plant bed outer boundary.

The experiments conducted to examine the effects of depth on littoral flow rates were performed in beds dominated by S. subterminalis at 2- and 4-m depths. In these experiments, mean flow rates for corresponding within-bed locations were not significantly different while, in contrast, the outside-bed flow rates were significantly different. These outside-bed flow rates differed widely between experiments (Table 4). Similarly, in the experiments examining the effect of dominant species on littoral flow rates, outside-bed flow rates were significantly different but within-bed flow rates for corresponding locations were not significantly different (Table 5). It should be noted, in the species comparison, depth was confounded with species because the P. illinoensis and S. subterminalis beds were at slightly different depths: 1.5- and 2-m depths, respectively. However, the similarity of within-bed flow rates among depths and species suggests that these factors (depth and species) did not have a large affect on within-bed flow rates. In addition, submersed plant surface area, which was over 3-fold greater in the S. subterminalis than in the P. illinoensis bed, also did not have a large affect on within-bed flow rates. The importance of depth and species can not be completely dismissed because a multifactor covariate analysis of the data set, exclusive of the outside-bed locations, also showed all factors to be significant (Table 6). The large data set used in the multifactor covariate analysis has provided power to detect subtle differences in model factors.

In absolute terms, the differences in within-bed flow rates within locations or among beds were very small. However, boundary layer thickness is an inverse square root function of flow rate (LBL equation), and small changes in low speed flow rates result in large

Table 6. Multifactor covariate analysis of within-bed location flow rates using a 60-second interval subset of the Lawrence Lake data set. $P < 0.001$ ***

Sources of Variation	df	F value
Depth	2	324.22 ***
Species	1	389.70 ***
Location	6	390.96 ***
Wind direction	1	33.02 ***
Wind speed	1	150.79 ***

differences in boundary layer thickness. Calculated Reynolds numbers (Re) for the slowest mean, mean for the study, and maximum mean within-bed flow rates, equaled 0.3, 0.7, and 4.6, respectively, at a distance 1 mm from the leading edge of a leaf. According to Vogel (1981), estimation of boundary layer thickness with this LBL equation is not dependable for $Re < 100$. Bearing this in mind, estimates of the momentum boundary layer thicknesses equal 9.1 mm, 6 mm, and 2.3 mm, respectively, for the slowest mean, mean for the study, and maximum mean within-bed flow rates. A flow increase from the slowest to average mean flow rate would result in a 34% decrease in boundary layer thickness, and an increase from the slowest to the fastest mean would result in a decrease of 75%. In a relative sense, at least, this indicates that small absolute changes in littoral flow rates would result in large changes in boundary layer thickness (Figure 5). These boundary layer thicknesses, however, are many times the submersed macrophyte leaf thicknesses themselves (<1 mm).

All experiments with relatively rapid within-bed flow rates were conducted in the late autumn and winter period when the mixed layer was deep or the lake was isothermal. The degree of thermal resistance to mixing is likely to have an affect on within-bed flow rates. In the fall, basin stability decreases, and wind energy is more readily

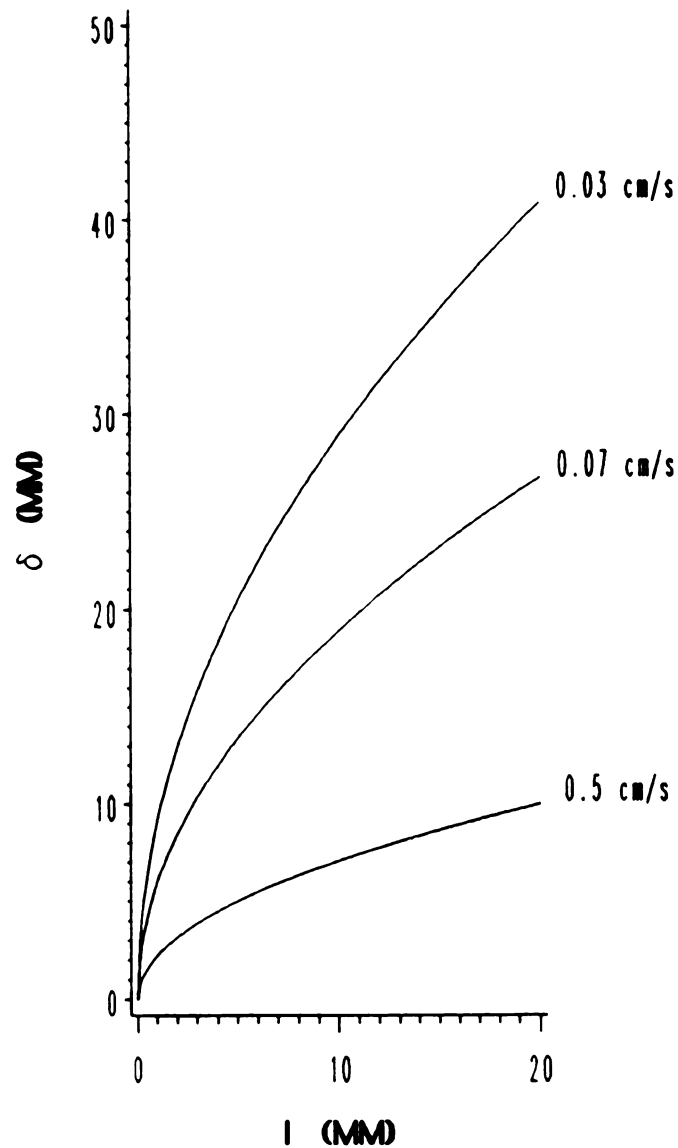


Figure 5. Theoretical momentum boundary layer development over a flat surface for the minimum mean, mean for the study, and maximum mean flow rates. δ = boundary layer thickness, l = distance from the leading edge.

transformed into currents, which circulate within the basin at relatively high rates. During the course of this study, rapid within-bed flow rates were rare: $>0.25 \text{ cm s}^{-1}$ occurred only 0.8% of the time. This percentage was only slightly biased in two ways: 1) it was determined simply by totalling rates for all experiments in the study, and most of these took place during the stratified period, and 2) the high flow rate experiment dates were chosen for their high wind conditions to determine the upper limit to littoral flow rates. Coincident with the higher autumn flow rates was a decrease in water temperature. The increase in water density with a decrease in temperature is more than offset by an increase in dynamic viscosity resulting in an increase in kinematic viscosity of $\approx 78\%$ for a change from 20°C to 0°C . The increase in viscosity counteracts the increase in autumn littoral flow rate and results in a net increase in boundary layer thickness. The general increase in boundary layer thickness would be accompanied by a decrease in shear at the M-EP surface and may be a part of the explanation for the increased epiphytic periphyton biomass noted during early winter and spring (e.g. Burkholder and Wetzel 1990).

The relationship between littoral flow rates, wind speed and direction, and depth and dominant species of submersed plant communities is complex. Wind speed and direction interact with lake stratification and basin morphometry to form the pattern of wind-driven currents and determine the depth of wave action. On the other hand, within-bed flow rates are affected to a great extent by the interaction of flowing water with the entire plant community, not simply from the summation of drag for individual plants. When flowing water encounters a submersed plant bed, a portion of the water is diverted over and around it (Fonseca et al. 1982). The proportion of diverted water is a function of flow rate, plant biomass, shape, and orientation behavior with respect to the direction and rate of flow. S. subterminalis leaf blades were observed to remain erect and still in flows $\leq 0.5 \text{ cm s}^{-1}$. As flow increased above this rate, the blades began to sway. A transition occurs where

the blade oscillations increase in amplitude biased in the direction of flow. At a rate of $3-6 \text{ cm s}^{-1}$, the blades bent and remained with their broad sides approximately parallel to the sediment and the leaf tips pointed in the direction of flow. As flow increased to $\approx 6 \text{ cm s}^{-1}$, the blades rapidly undulated in the current. It should be noted that only leaf blades in the outer portion of the canopy exhibited these behaviors, and the distance into the bed affected was a function of flow rate. In Experiment 4, the flow rate above the S. subterminalis canopy was $\approx 30 \text{ cm s}^{-1}$, yet the within-bed flow rates were $< 0.5 \text{ cm s}^{-1}$. Apparently, when the leaf blades of the outer canopy were bent in the direction of flow, they formed an effective barrier and flow was diverted over the top of the macrophyte community. This diversion of water around a macrophyte bed is probably a step function or nearly so, with an abrupt decrease of within-bed rates as submersed plant leaves are deflected so that their broad surfaces are parallel to the direction of the flow. The leaves may then form a quasi-interlocked barrier to flow into the bed.

The multifactor covariate analysis and multiple comparisons, taken together, suggest that differences occur in flow rate pattern resulting from differences in dominant species, depth, and location within a plant bed, but are subtle. Substantially more important is the fact that the plants form beds. As observed in this study and illustrated in the scenario above, within-bed flow rates are greatly reduced even at low plant densities. These observations beg the question of what plant bed density is optimal for a submersed plant species. It is valid to address this as a species rather than a community level question because these submersed plants often form nearly monospecific stands in nature. The repercussions for a plant as a member of a submersed plant bed include reduced flow rates and increased diffusive resistance, but protection from shear under rapid flow rates.

Rapid fluctuations occur in littoral flow rates (Figure 6). The flow rate versus time signal is the summation of several signals of

various periods and amplitudes. These signals include 1) unidirectional flow, wind or convection driven currents, 2) circular with a transition to reciprocating motion driven by wave action, and 3) animal induced movement. The rapid, though small, fluctuations in flow presented in Figure 6 suggest that submersed plant boundary layers may be unstable. The concentration gradient is, therefore, a time-averaged function, constantly integrating the concentration at the M-EP surface, under metabolic or physicochemical control, with the bulk phase concentration under hydrodynamic control.

The large boundary layer resistance to diffusion, coupled with a high concentration of micro- and macrophyte photosynthetic cells and tissue, make the submersed M-EP complex a unique environment. Physically, the microenvironment is highly dynamic because of photosynthetic oxygen production to supersaturating levels, removal of inorganic carbon, and shifts in pH. The cycle is diurnal with dark consumption of oxygen and increased production of CO_2 . The boundary layer acts to maintain an elevated concentration of products within the community and surrounding region. For example, internal lacunar gas space storage of CO_2 in submersed angiosperms is maximized at night. The high concentration of juxtaposed autotrophic and heterotrophic organisms results in a tight coupling of regenerated nutrients (Wetzel 1990). Once nutrients enter the M-EP complex, boundary layer resistance to diffusive transport and rapid turnover rates will tend to retain these nutrients within the complex. This retention is indicated in a simple sense by the rapid accumulation of material in littoral zones, even in lakes with little particulate influx in streams and rivers. Moeller et al. (1988) concluded that epiphytic uptake of phosphorus from the open water ultimately helps to sustain the apparently independent phosphorus cycle of rooted macrophytes, by increasing phosphorus deposition as littoral sediments. This accumulation of organic matter and nutrients is similar to early successional stages on mineral soils as noted by Olson (1958). The pioneer dune species provided and trapped

S. subterminalis, 2m depth

wind = leeward, 4.8m/s

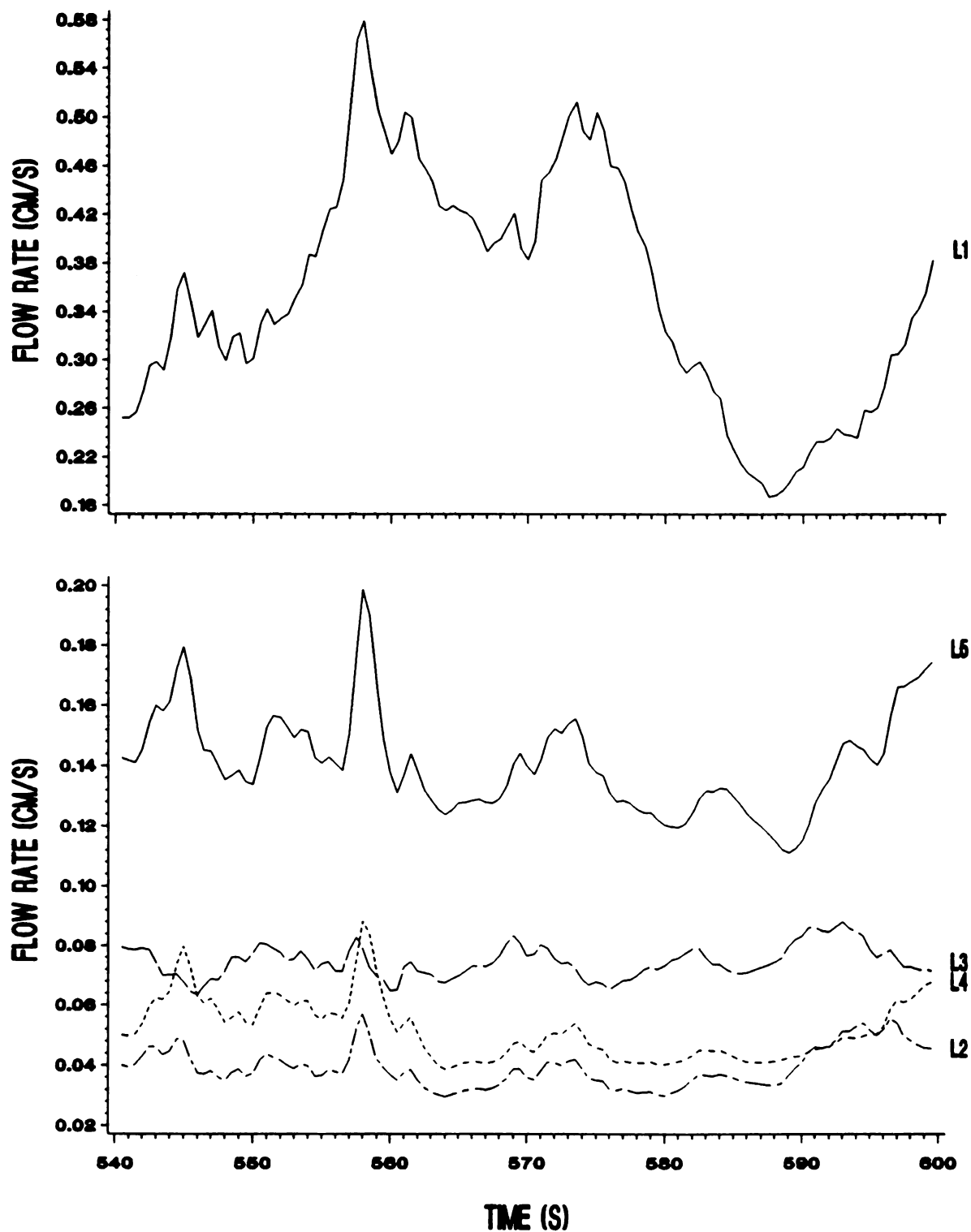


Figure 6. Typical flow rate versus time plot for Experiment 8, 0.5 second measurement interval (see Figure 2 for probe locations).

organic detritus that directly retained nutrients (most importantly, nitrogen), incorporating them into the soil and biomass. Uptake and retention within the M-EP complex introduces an additional temporal component to the passage of dissolved matter through the aquatic ecosystem and will affect community structure, both spatially and temporally. In addition, retention of environmental contaminants (particularly organic) in the physicochemically extreme and dynamic M-EP complex may be important in the natural alteration and decomposition of these compounds.

CHAPTER 2

SUBMERSED MACROPHYTE-EPIPHYTIC PERIPHYTON MICROSCALE FLOW PATTERNS

INTRODUCTION

Flow rates within submersed macrophyte communities are slow, resulting in very small Reynolds numbers (Re) for submersed plant surfaces (Chapter 1). These small Re indicate that flow associated with submersed surfaces is laminar, in which case transport across the water column/macrophyte-epiphytic periphyton (M-EP) interface must be via molecular diffusion. However, a solution has not been found to the theoretical problem of flow stability for steady flow past a body of finite dimension (Happel and Brenner 1973).

I define stable flow as flow without separation or turbulence. Separation is the formation of a vortex associated with flow around a body. The vortex may form up- or downstream of the body or feature of the body causing the separation. Empirically determined critical Re values for the onset of unstable flow are of the order of 10-100. There is a tendency for separation to occur at lower Re for non-streamline bodies. For example, separation occurs for a cylinder oriented perpendicular to flow at $Re = 34$, and for a sphere at $Re = 17$ (Happel and Brenner 1973).

The vortex formed at the point of separation moves bulk water along the z -axis (perpendicular to flow), and transports gases and dissolved substances more rapidly across the water column/submersed surface interface than would occur by molecular diffusion alone. There remains a region, between the M-EP surface and the vortex, where transport is via molecular diffusion. Therefore, where separation occurs in flow around the M-EP complex, the concentration gradient (dC/dz) of Fick's first law of diffusion will be steeper than the case with no separation.

Thus, the diffusive path length decreases for the region of the surface near the point of separation.

Vogel (1981) warns that predictions of laminar flow boundary layer (LBL) thickness (δ), from $\delta = 5lRe_l^{-1/2}$ or $\delta = 5(\nu l/U)^{1/2}$ for $Re < 100$ are unreliable. From Chapter 1, the flow rate within submersed macrophyte communities is virtually always slow enough and plant geometry sufficiently complicated that current theoretical understanding of low Re hydrodynamics fails to predict reliably microscale flow patterns or δ around submersed plant leaves. Since diffusive boundary layer (DBL) development is a function of microscale flow patterns, it is imperative that these patterns be empirically determined as part of the effort to elucidate the relationship between microscale hydrodynamics and transport across the water column/M-EP interface.

The objectives in this component of the study were to determine the pattern and rates of flow around the submersed M-EP complex for various flow rates, water temperatures, and M-EP complex conditions (i.e., orientation, presence or absence of epiphytic periphyton, and species of macrophyte) with regard to LBL development.

MATERIALS AND METHODS

Flow patterns were visualized surrounding submersed macrophyte leaves, in a laboratory flume, using two techniques: videography and time-lapse photography. Figure 7 is an illustration of the flume and camera setup. The flume had a working section of 1-m, was 27-cm wide, with a water depth of approximately 26 cm. Flow rate in the flume was regulated by the number of centrifugal pumps used to circulate water and by adjusting a gate valve on the input to the upstream end of the flume. To smooth flow, six flow collimators were placed upstream of the working section and two downstream. The collimators were made from fluorescent light diffusers with 1.6-cm square openings, 1.4-cm deep. The furthest upstream collimator was covered with several layers of offset nylon window screen, which acted as a diffuser equalizing flow over the cross

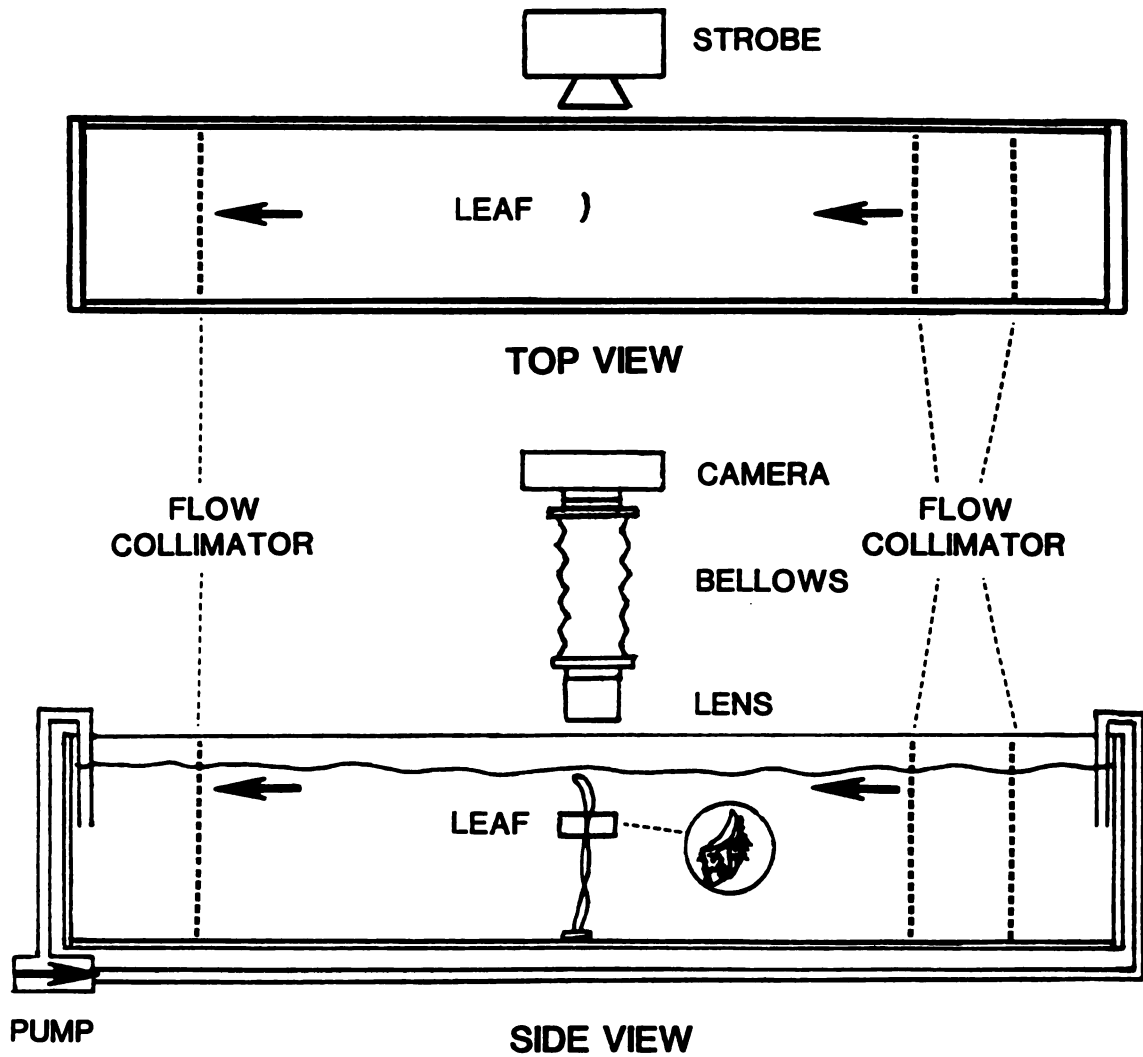


Figure 7. Flume and camera setup for video- and time-lapse photography of flow around submerged macrophyte leaves. See text for explanation.

section. To facilitate temperature regulation, the flume was insulated with foam insulation board. For the low temperature experiments, the water was circulated through an ice bath. Flow in the working section of the flume retained some small scale turbulence similar to that found within lake littoral macrophyte communities (eddies millimeters to centimeters in diameter, Chapter 1). Waves were induced in the flume by rhythmically (in phase) displacing water at the upstream end of the flume.

Videography was utilized to record streaklines formed as a dye trail flowed around a leaf or through a collection of leaves. Methyl blue and milk were used as the dye. Milk was superior because its buoyancy closely matches that of water and it provided a greater contrast in the monochrome video image. A time-lapse photographic technique of neutrally buoyant particles was adapted from Ackerman (1986) to record pathlines and to measure flow rates in a narrow focal plane of the region surrounding the submersed leaf cross section parallel to flow.

The dye and neutrally buoyant particles were dispensed upstream of the leaf with a hypodermic needle attached to a 5-ml disposable pipet. The long, narrow shaft of the pipet and needle minimized disturbance of the flowing water. The dispensing syringe was fitted with a fine-thread screw device that facilitated the slow, smooth depression of the plunger when manually turned; this permitted the dye or particles to be dispensed at a rate matching flow (i.e., the screw device was turned at a rate that maintained the dye stream at the width of the needle with no dilution of the dye or, conversely, displacement of the water by excess dye). Submersed macrophyte leaves were held in a clamp, located on or near the floor of the flume, and were positioned at mid depth such that the leaf was viewed in cross section from above. The time-lapse photographs were taken with a 35-mm camera with a bellows attachment that provided 0.5 to 3x magnification and a narrow focal plane. Kodak Tri-X Pan film, pushed during development to ASA 1600, was used (Acufine

developer, Acufine Inc., for 10 minutes). The neutrally buoyant particles were heat-denatured albumin (hard-boiled egg white), which ranged in diameter from 60-200 μm . The strobe was positioned 90° to the camera, illuminating the leaf through the flume's clear acrylic side wall.

The pathline for a particle, as it traversed the field of view in the focal plane of the camera, was recorded as multiple exposures on a negative film frame. The distance between particle exposures on the film was a function of magnification, flow, and flash rate. The strobe flash rate was selected as a compromise between spatial resolution and accuracy of flow rate measurements. The shorter the interval between flashes the greater the spatial resolution of measurements; conversely, the longer the interval between flashes the greater the distance between particle exposures and the more accurate the distance measurement.

The video recordings and time-lapse photographs were analyzed for the occurrence of unstable flow. Unstable flow was marked by separation, the occurrence of vortices associated with the plant surfaces.

The coordinates of exposed particles on a film frame were digitized as sequential pairs for a particle as it traversed the field of view. All measurements were made relative to the coordinates of the leaf cross section. Flow rate was calculated for the mean coordinates of paired points as the distance traveled during the flash interval divided by the duration of the interval. One to several frames were combined to provide flow rate measurements over as much of the field of view as possible for an experiment.

Flow rates were estimated for the region surrounding the leaf cross section and for profiles extending from the leaf surface perpendicular to flow, as well as up- and downstream, utilizing regionalized variable theory or geostatistics (Webster 1985, Robertson 1987, Gamma Design Software 1991). In the initial step of the geostatistical procedure, described in Chapter 1 for the one-dimensional case, the semivariance

statistic was found for the measured flow rates of an experiment and fitted to a spherical model. The spherical model provided a robust fit for the semivariograms of all experiments, resulting in $r^2 > 0.90$ (Figure 8). The kriging procedure provided precise, unbiased flow rate estimates surrounding a leaf cross section and an estimate of variance (Robertson 1987). While a small amount of anisotropy often existed in the data for an experiment, comparison of jackknife analyses of kriged estimates of flow rate for isotropic and anisotropic models revealed that the anisotropic model did not greatly improve the fit of estimated flow rate values to measured values over the isotropic model. The lack of improvement of fit when the anisotropic model was used was a result of the large number of evenly distributed flow rate measurements. Because of the number and distribution of measurements in these experiments, each estimate of flow rate was made using nearby neighbors where the impact of anisotropy is minimal. In the kriging procedure, zero flow rate values were added to the experimental data set for coordinates within the leaf cross section area to yield an estimated contour of 0.0 cm s^{-1} corresponding to the leaf cross section outline. These added data force the flow rate profiles to zero at the leaf surface, as is the case in nature because of the 'no-slip' condition at the surface. Of primary interest in this study are the flow rate values at some distance from the M-EP surface where flow rates approach the free stream velocity (U). At this distance from the M-EP surface, the 0 cm s^{-1} flow rate values added to the leaf cross section had no affect on the estimate of flow rate.

To estimate δ , a spherical model was fit to the kriged flow rate profile data using a non-linear regression technique (SAS Institute, 1990). This spherical model [flow rate = $U(1.5(z/Z) - 0.5((z/Z)^3)$ where, U is free stream flow rate, z is distance from the M-EP surface, and Z is the distance z where du/dz approaches 0, the asymptote] was chosen because it provides a parameter that estimates the free-stream flow rate (U), and a second parameter that estimated the distance (z)

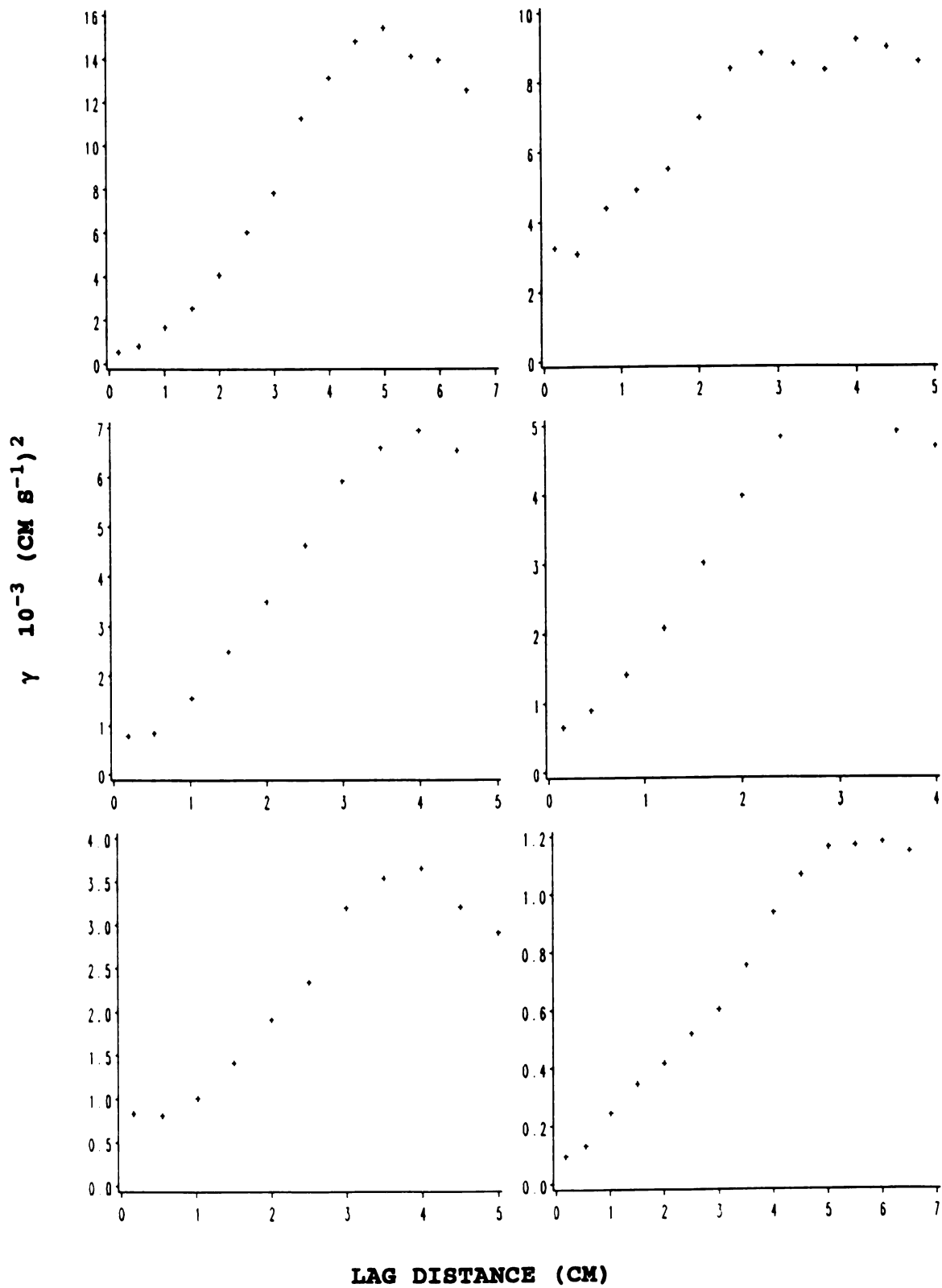


Figure 8. Semivariograms of flow rate in the plane parallel with flow for Experiments 1 through 6.

from the M-EP surface where $du/dz=0$, the boundary layer thickness. The model fit was good for all profiles perpendicular to flow ($r^2 > 0.90$).

RESULTS

Flow Stability

Analysis of video recordings of flow around S. subterminalis leaves revealed unstable flow associated with the leaf only when a reciprocal (wave-induced) motion was superimposed over a rapid, 2 cm s^{-1} , unidirectional flow. Separation events were brief, occurring only at the moment when the leaf reversed direction and moved against the unidirectional flow. This moment was the instant of maximum relative flow rate. In addition, when leaf density (leaves per horizontal cross section) of S. subterminalis was increased from a single leaf in the flume to $\approx 0.5 \text{ leaves cm}^{-2}$ (the approximate *in situ* density in Lawrence Lake) flow instability associated with a leaf surface was not enhanced; rather, turbulent eddy size decreased for the water flowing through the leaves.

Unstable flow was found associated with the P. praelongus leaf. The separation occurred on the downstream side of the leaf tip, that portion of the leaf oriented perpendicular to the direction of flow (Figure 9, upper panel). This form of separation, known as viscous entrainment, was characterized by a slow cyclic rotation and did not display the chaotic pattern associated with more vigorous separation and turbulence. Separation did not occur on the downstream side of the undulate portion of the leaf. The P. praelongus leaves form a U-shape in lateral cross section. When the leaf was oriented so that the long axis was perpendicular and the short axis parallel to flow, again, no separation was observed (Figure 9, lower panel).

Figure 9. Time-lapse photograph of flow pathlines around a P. praelongus leaf. Flow is from right to left, $\approx 0.42 \text{ cm s}^{-1}$, 200 flashes min^{-1} . Upper panel viewed in longitudinal cross section. Note the arching pathline downstream of the leaf tip. Lower panel viewed in lateral cross section.

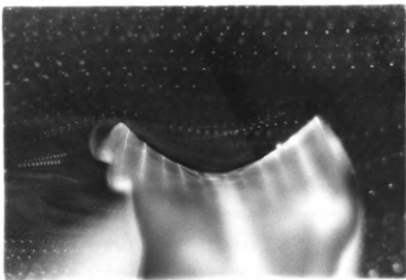


Figure 9.

Microscale Flow Patterns and Rates

The shape of the isotropic semivariogram for the two-dimensional spatial data for the microscale flow rate experiments indicate that autocorrelation of flow rates occurred at distances <7.6 cm, slightly more than half the distance across the full field of view (Figure 8). In all but two experiments the "nugget" variance (variance over the distance of the smallest lag-distance class) was less than 1% of the population variance which suggested that spatial autocorrelation at the 0-7.6 cm scale accounts for the variation in flow rate and that there was very little measurement error. The nugget variance was 26% and 7% of population variance for Experiments 2 and 5, respectively. There is no known difference between experiments in the manner flow rates were measured. Therefore, it is likely the nugget variance of Experiments 2 and, to a lesser extent, Experiment 5 was the result of autocorrelation at distances less than the shortest distance between measurements rather than measurement error.

Figures 10 through 15 show the isopleths of flow rate (upper panel) and standard deviation (lower panel) estimates in the plane of flow surrounding a S. subterminalis leaf viewed in lateral cross section. Flow is from right to left, and the presence or absence of epiphytic periphyton and water temperature are noted in the figure captions. Note that the error is small and uniform over the cross section. In all experiments the pattern of flow was similar. The M-EP complex had a region of reduced flow that extended a long distance downstream (>2 cm), a comparatively short distance to the sides of the complex (perpendicular to flow), and an intermediate distance upstream. The estimated boundary layer thicknesses (δ) (Table 7, Figures 10-15), which were based on the kriged estimates of flow rate along a profile extending out from the leaf and perpendicular to flow, asymptotically approached the free-stream velocity as predicted by the Navier-Stokes equation (Vogel 1981).

In general, flow rate shows an inverse relationship with δ (Table

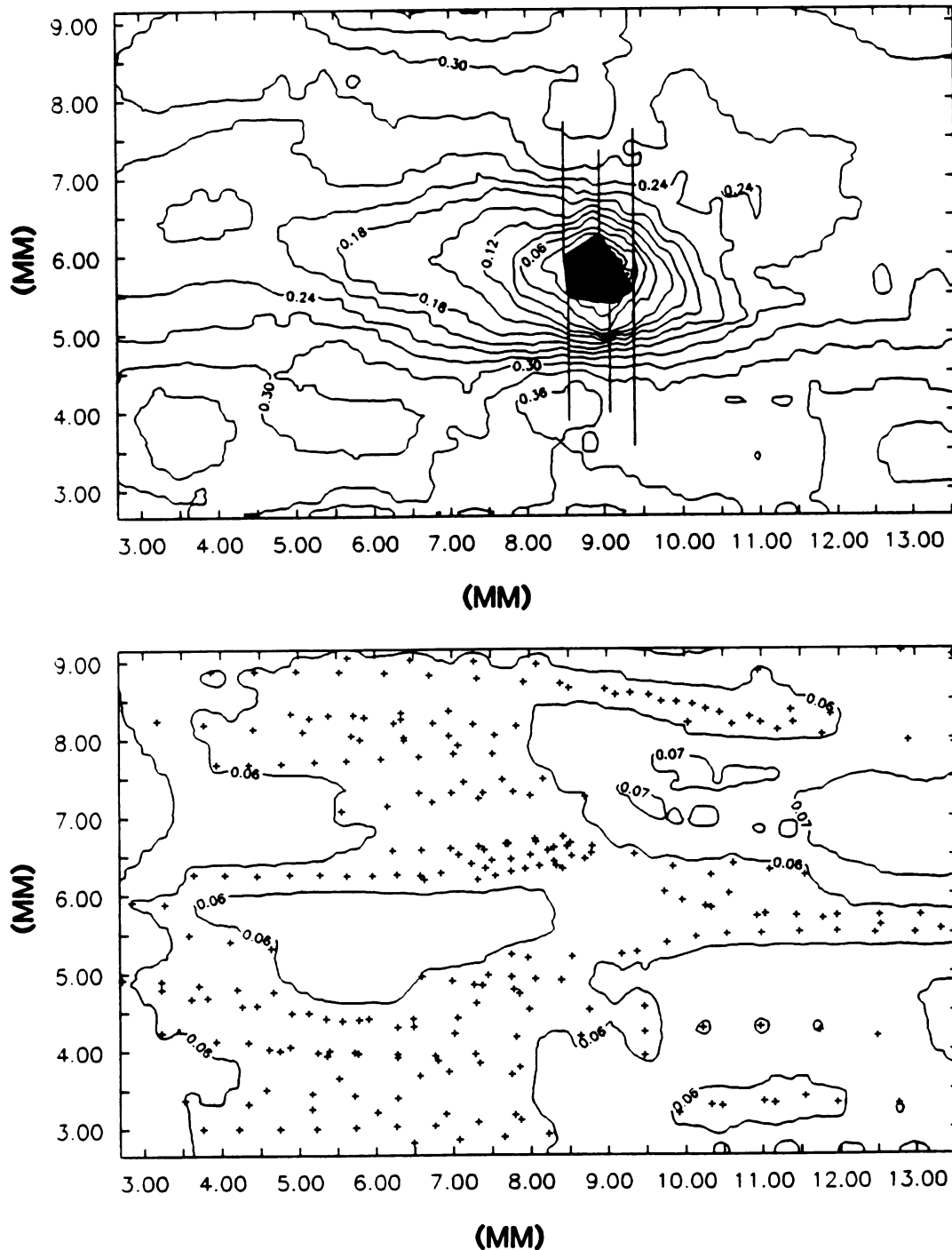


Figure 10. Experiment 2 isopleth of estimated flow rate (upper panel) or standard deviation (lower panel) in the plane parallel to the direction of flow around a *S. subterminalis* leaf viewed in lateral cross section. The solid lines projecting perpendicular to flow in the upper panel are the estimated δ . Flow is from right to left, rate in cm s^{-1} , epiphytic periphyton present, and water temperature 23°C .

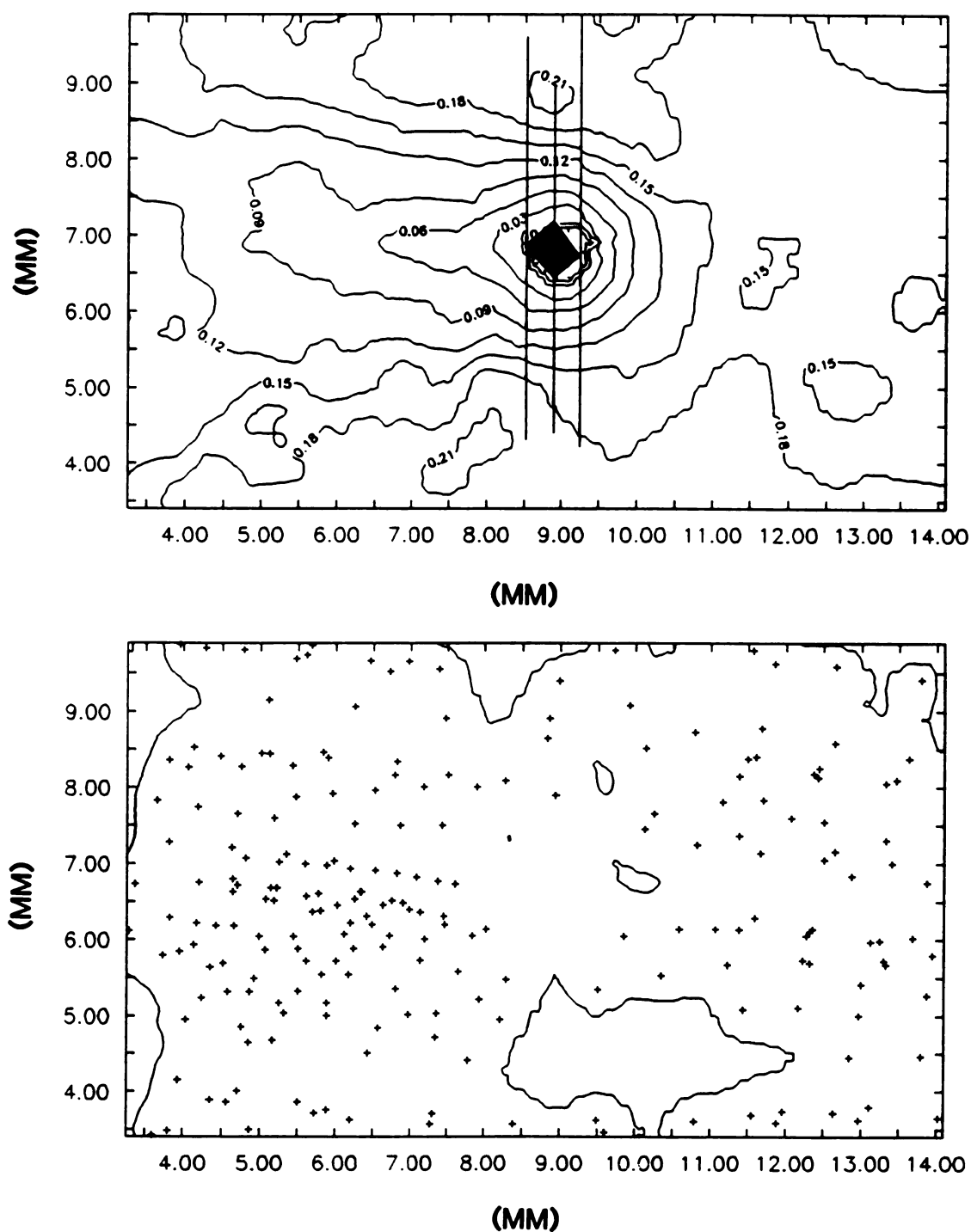


Figure 11. Experiment 5 isopleth of estimated flow rate (upper panel) or standard deviation (lower panel) in the plane parallel to the direction of flow around a *S. subterminalis* leaf viewed in lateral cross section. The solid lines projecting perpendicular to flow in the upper panel are the estimated δ . Flow is from right to left, rate in cm s^{-1} , epiphytic periphyton present, and water temperature 23°C .

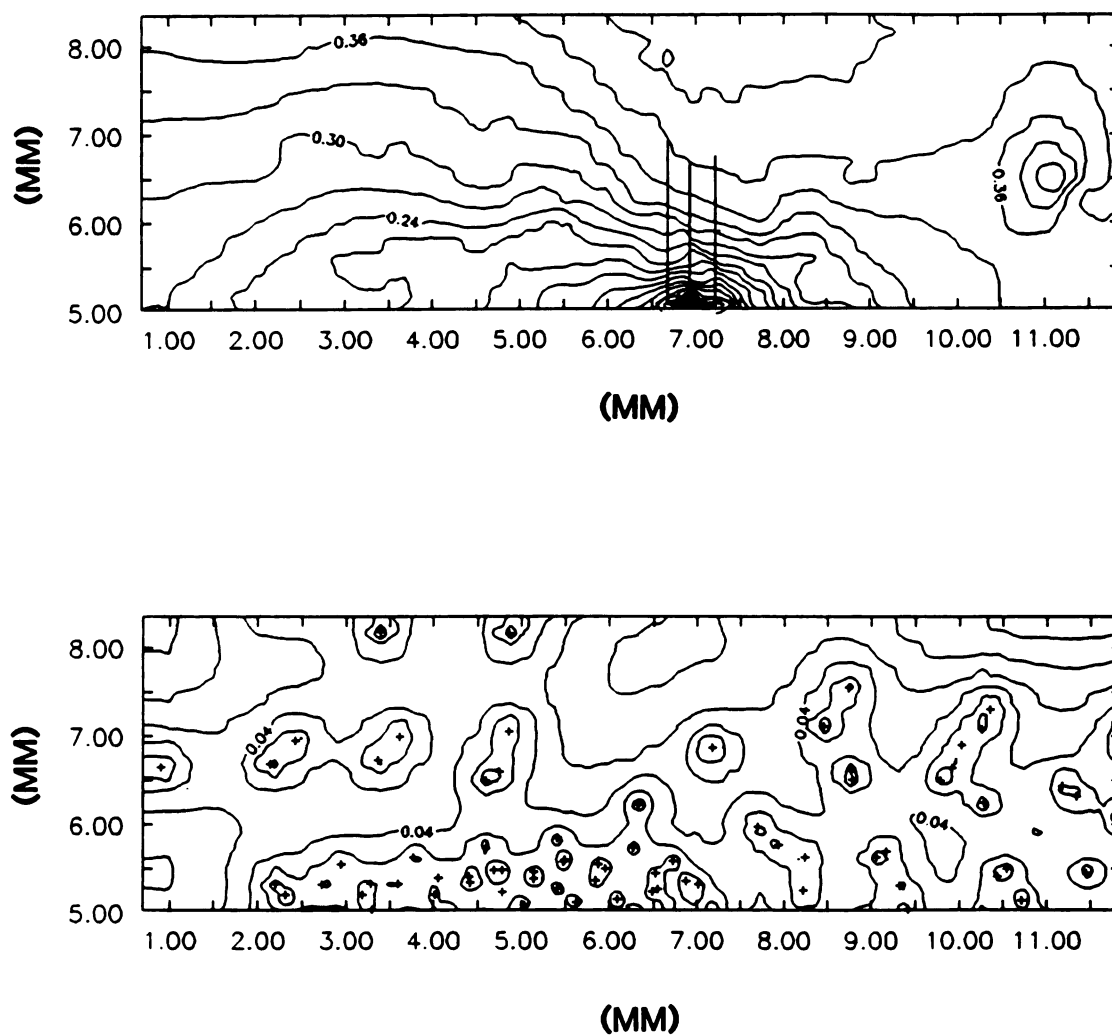


Figure 12. Experiment 1 isopleth of estimated flow rate (upper panel) or standard deviation (lower panel) in the plane parallel to the direction of flow around a *S. subterminalis* leaf viewed in lateral cross section. The solid lines projecting perpendicular to flow in the upper panel are the estimated δ . Flow is from right to left, rate in cm s^{-1} , epiphytic periphyton present, and water temperature 6°C .

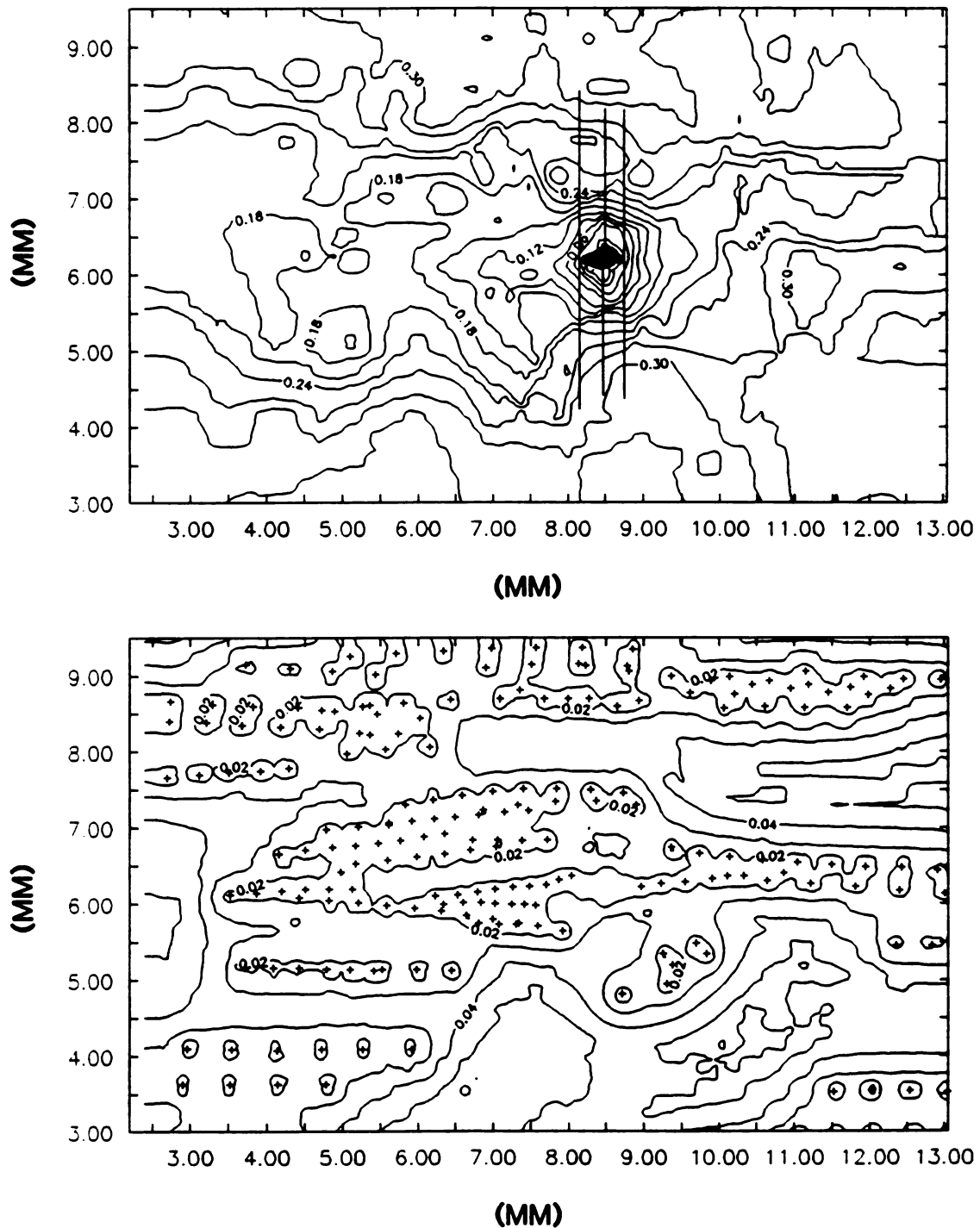


Figure 13. Experiment 3 isopleth of estimated flow rate (upper panel) or standard deviation (lower panel) in the plane parallel to the direction of flow around a *S. subterminalis* leaf viewed in lateral cross section. The solid lines projecting perpendicular to flow in the upper panel are the estimated δ . Flow is from right to left, rate in cm s^{-1} , epiphytic periphyton absent, and water temperature 23°C .

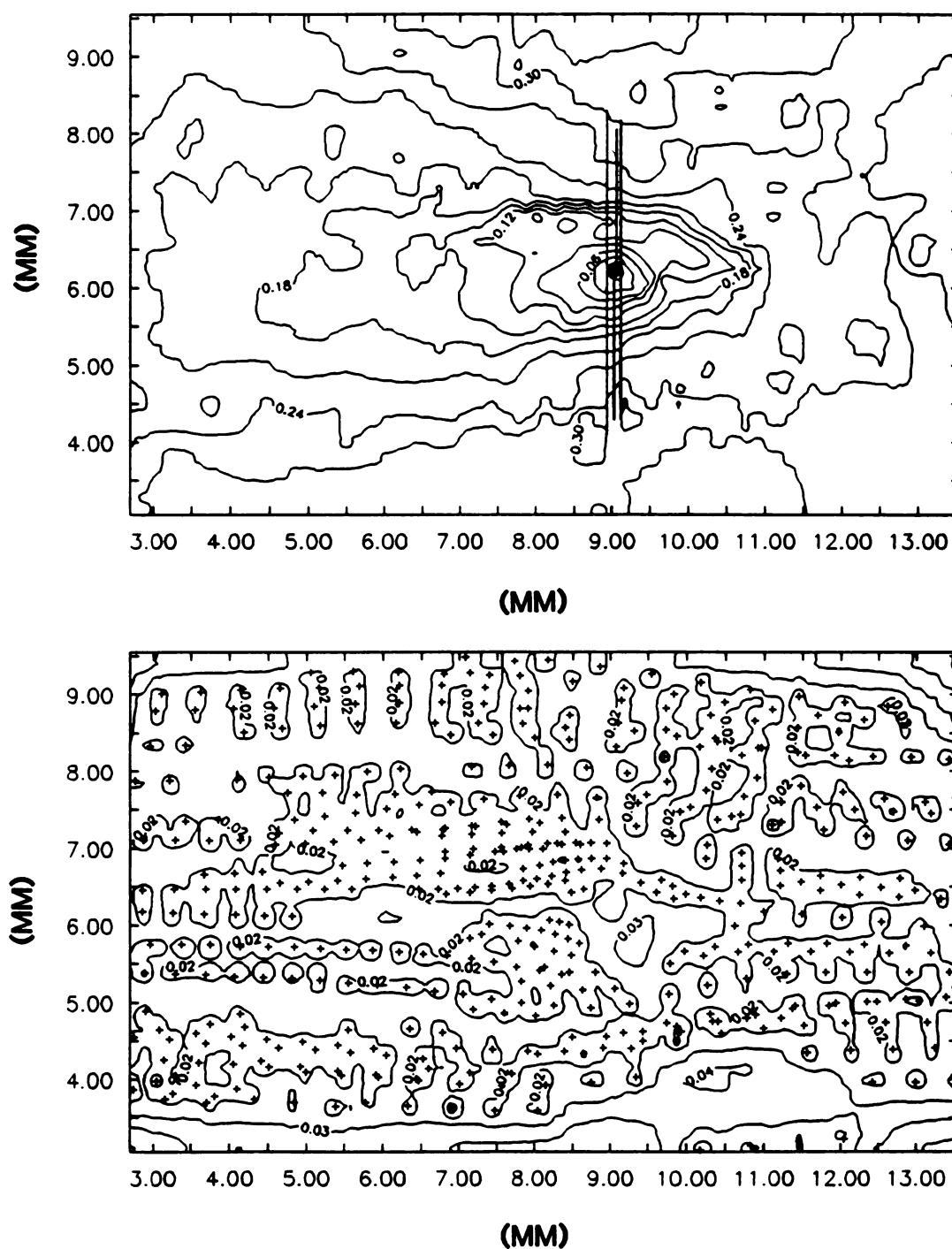


Figure 14. Experiment 4 isopleth of estimated flow rate (upper panel) or standard deviation (lower panel) in the plane parallel to the direction of flow around a *S. subterminalis* leaf viewed in lateral cross section. The solid lines projecting perpendicular to flow in the upper panel are the estimated δ . Flow is from right to left, rate in cm s^{-1} , epiphytic periphyton absent, and water temperature 7°C .

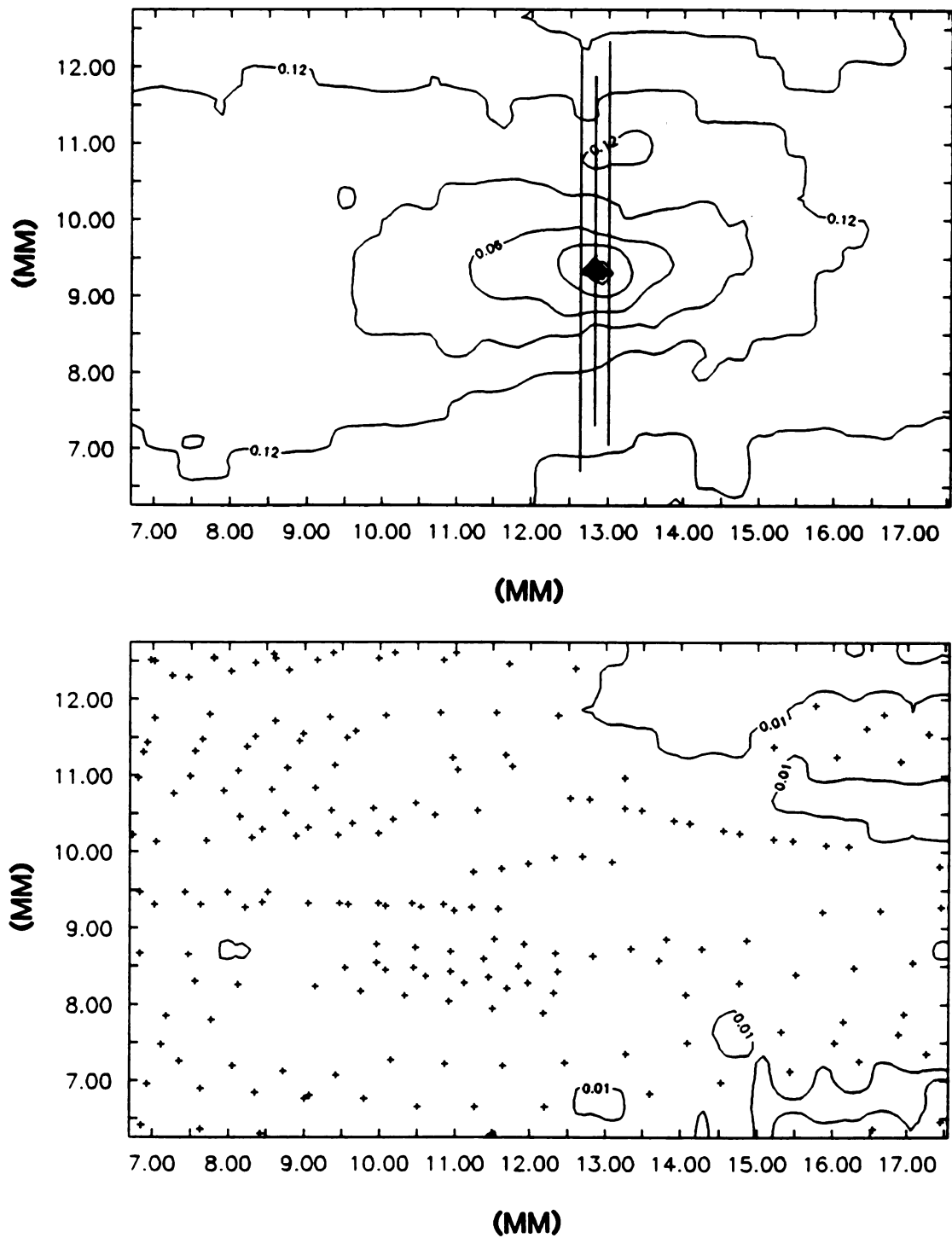


Figure 15. Experiment 6 isopleth of estimated flow rate (upper panel) or standard deviation (lower panel) in the plane parallel to the direction of flow around a *S. subterminalis* leaf viewed in lateral cross section. The solid lines projecting perpendicular to flow in the upper panel are the estimated δ . Flow is from right to left, rate in cm s^{-1} , epiphytic periphyton absent, and water temperature 5°C .

7). This relationship is further illustrated by comparing two experiments. M-EP complex size and water temperature are nearly the same for Experiments 2 and 5, with flow rate 0.1 cm s^{-1} faster in Experiment 2. As expected, measured δ was much larger for the slower flow rate of Experiment 5.

When epiphytic periphyton was present on the leaf the M-EP size was much larger than when it was absent (cf. Figures 10-12 and Figures 13-15, periphyton present or absent, respectively). However, contrary to the predictions from the boundary layer thickness equation, δ were usually larger when periphyton was absent (Experiments 3, 4, 6) than when present (Experiments (1, 2, 5) (Table 7). The exceptional case was Experiment 6 (Figure 15) where periphyton was absent yet δ_{pred} was greater than δ . In Experiment 6 the leaf was oriented at an obtuse angle to bulk flow which contributed to producing a δ less than predicted.

As a further illustration of the effect of leaf size and orientation to the direction of flow on δ , compare Experiments 1 and 2. The flow rate was higher in Experiment 1 (0.42 cm s^{-1}) than in 2 (0.33 cm s^{-1}) and the M-EP complex was larger in 2 than in 1. Therefore, δ was expected to be larger for Experiment 2. However, the measured δ was larger for Experiment 1 than 2. While periphyton was present on both leaves, the leaf in Experiment 2 was oriented at an obtuse angle to flow.

Flow rates were the same for Experiments 3 and 4 where periphyton was absent and the leaves were oriented parallel to flow. However, leaf size in Experiment 3 was more than twice that of Experiment 4 while water temperature was much greater in 3 than 4. The predicted δ and average δ were equal for these experiments as the larger leaf size of Experiment 3 was offset by the lower temperature in Experiment 4 (Table 7).

Table 7. Summary of the *S. subterminalis* microscale flow pattern experiments. δ is the average and δ_{pred} the predicted distance z from the surface where du/dz approached 0 for the region perpendicular to flow. U is the free stream velocity and l is the average of the length and width dimensions for the cross section.

Expt #	Figure #	Epiphytic Periphyton	U (cm s ⁻¹)	l (mm)	Temperature (°C)	δ_{pred} (mm)	$\delta \pm 95\%$ CI (mm)
1	12	+	0.42	0.54	6	2.4	1.67 \pm 0.085
2	10	+	0.33	0.85	23	2.5	1.48 \pm 0.142
3	13	-	0.30	0.45	23	1.9	1.90 \pm 0.098
4	14	-	0.30	0.18	7	1.9	1.93 \pm 0.078
5	11	+	0.20	0.75	23	2.9	2.42 \pm 0.172
6	15	-	0.16	0.44	5	3.5	2.46 \pm 0.131

DISCUSSION

Flow Stability

Flow separation, when it occurs associated with the macrophyte-epiphytic periphyton (M-EP) surface, may have two effects. If the vortex formed at the point of separation has sufficient force, the shear stress at the M-EP surface will erode periphyton. If the vortex is less forceful, the result is to greatly increase the transport of gases and dissolved substances across the water column/M-EP interface without eroding periphyton. When flow separation occurs, the cycloid movement of water within the vortex transports dissolved substances across the plane parallel to the M-EP surface (i.e., along the z-axis, or perpendicular to the M-EP surface) more rapidly than via molecular diffusion alone. However, as a result of the "no-slip" condition, there remains a layer of water of finite thickness over the M-EP surface where there is no bulk water movement along the z-axis, and transport across this layer, reduced in thickness by the vortex, is via molecular diffusion.

The results of this study, on natural material which has complex form, and of studies performed under highly controlled conditions indicate that 1) separation can occur at very low Reynolds numbers (Re) (i.e., small size and slow flow rate), and 2) vortex formation is a function of the degree of free-stream turbulence, rate of flow, and a complex form factor (Happel and Brenner 1973, Leyton 1975 and Van Dyke 1982). The form factor accounts for the effect of size, shape and orientation in combination. In this study, separation was induced only at a high flow rate ($>2 \text{ cm s}^{-1}$) for the small ($\approx 0.9\text{-mm}$ wide) S. subterminalis leaves. Separation was found for the larger ($\approx 10 \times 3 \text{ cm}$) P. praelongus leaf at a moderate to fast flow rate ($\approx 0.4 \text{ cm s}^{-1}$). For flow rates commonly found within beds, the minimum leaf size where separation occurs is between the sizes of these two macrophytes. For a leaf smaller than this minimum, the complexity of the M-EP form (i.e., leaf orientation, shape or periphyton configuration) is much less

important, because separation does not occur except for very rare circumstances.

When flow rate is sufficient for separation to occur, size alone is inadequate as a predictor of separation. The shape of the M-EP complex is also important. At low Re , separation occurs when a body has a structure with a relatively large ratio of surface projecting perpendicular versus surface parallel to flow up- or downstream of the projecting structure. This point was observed in the time-lapse photographs of flow around a *P. praelongus* leaf where separation occurred downstream of the leaf tip (Figure 9, upper panel). However, in the same photograph it can be seen that no separation occurred downstream of the leaf undulations. The surface that projected perpendicular to flow at the leaf tip was very large compared to the leaf surface immediately downstream of the leaf tip and parallel to the direction of bulk flow. In contrast, on the upper surface of the leaf, the slope of the surface on the downstream side of the undulation is more gradual and no separation occurred. The role of shape in decreasing the occurrence of separation is further illustrated in the time-lapse photograph of the *P. praelongus* leaf oriented with its short axis parallel to flow (Figure 9, lower panel). While the slope on the upper surface of the curved leaf is quite steep, there is sufficient surface, downstream of the leading edge of the leaf, to prevent separation at this moderate flow rate.

As water temperature decreases, its kinematic viscosity (ν) increases. Therefore, for separation to occur at lower temperatures, higher flow rates, and/or sharper angles and greater surface area of projecting structures are required. It is less likely separation will occur at lower temperatures because of the greater viscosity of water. Periphyton erosion requires relatively high shear stress at the M-EP surface and, probably, only occurs at points of separation. The greater quantities of periphyton found in late fall, winter and spring (Burkholder and Wetzel 1990) may, in part, be accounted for by the

decreased occurrence of separation and accompanying high shear stress when water temperatures are lower.

In nature, separation is likely to occur only rarely for submersed plants with narrow leaves or leaflets, such as S. subterminalis or Myriophyllum species. Separation will occur, for these small leaves, only during rare high flow events in lentic systems (e.g., Experiment 4, Chapter 1), or in lotic systems. In either case, separation will only occur at the edge of the macrophyte bed because flow rate very rapidly decreases within the bed (Table 1), as does free-stream turbulence. When considering small-leaved submersed plants of an aquatic ecosystem, flow separation is an insignificant mechanism of transport across the water column/plant surface interface.

The occurrence of separation for larger leaved submersed plants, such as the broad-leaved Potamogeton species, is dependent on leaf orientation to flow direction, as well as flow rate. My observations of *in situ* Potamogeton species leaf orientation indicates that the leaves are randomly oriented rather than influenced by the direction of the prevailing current. When these plants occur in relatively dense stands where flow rates are greatly reduced, it is unlikely that separation is of much importance in reducing diffusive resistance across the water column/plant surface interface for the bed. However, these species are also found over-topping the canopy of shorter submersed macrophytes and on open sites with very low densities. In these cases, the flow rates would be much greater, and separation is likely to significantly decrease the diffusive resistance surrounding the leaves.

Given the above observations, it is likely that erosion events of epiphytic periphyton occur more frequently for broad-leaved than narrow-leaved plants. In addition, epiphytic periphyton is more likely to erode from broad-leaved submersed macrophytes colonizing open sites than in dense beds. Therefore, epiphytic periphyton density is expected to be lower in these open sites than within plant beds unless no relatively high flow events have occurred. In addition, macrophyte and/or

epiphytic periphyton primary productivity would be greater for the broad-leaved plants on open sites than for plants in beds, if all other conditions are equal. This last point may be important. Sediment nutrient and structural characteristics are generally superior within the boundaries of submersed plant beds as a result of accumulation of mineral and organic matter than are open sediments. Therefore, the more favorable diffusive transport conditions of open sites may not offset the greater fertility of sediments within plant beds.

Microscale Flow Patterns and Rates

When epiphytic periphyton was present, average estimated boundary layer thickness (δ) was less than the δ_{pred} ; while when periphyton was absent, average δ was less than the δ_{pred} in only one case and equal in the other two (Table 7). Note that δ perpendicular to flow is shortest at a point between the leading and trailing edges of the S. subterminalis-EP complex regardless of experimental conditions (Figures 10-15). This result is contrary to what would be expected for a fully developed laminar flow boundary layer (LBL) over a flat surface, in which case the δ would increase in thickness with increasing distance from the leading edge. The boundary layer equation contains parameters pertaining to size (l), flow rate (U) and viscosity (ν), but these are inadequate to describe boundary layer development in all cases. Some other factor must be important in determining the pattern of boundary layer development.

For low Re flow, such as found associated with the S. subterminalis leaves or over much of the surface of the large P. praelongus leaves, viscous forces dominate. As a result, separation does not occur and streamlines (a line to which the local direction of flow is everywhere tangent) do not cross (Vogel 1981). Upon encountering a small body, such as the S. subterminalis-epiphytic periphyton complex, flow is displaced around the body and shear stress at the surface (also known as skin friction) causes flow to decelerate (illustrated in Figure 16).

Because no separation occurs and streamlines do not cross, the displaced water flows through a constricted area adjacent to the side of the body. This point of minimum area available for displaced flow corresponds with the inflection point of flow streamlines around the S. subterminalis-EP complex. As flow is displaced around the body, streamlines converge upon approaching the inflection point, and since flow does not cross streamlines, the flow rate must increase. This inflection point in flow is also the point of maximum shear rate (flow rate gradient) and the minimum δ . Downstream of the inflection point, flow curves behind the body and streamlines diverge resulting in deceleration of flow.

The shear rate at the inflection point is dependent on the volume of water displaced by the projecting structure (compare left and right panels, Figure 16). As the volume of displaced water increases, the shear rate, or flow rate gradient, adjacent to the side of the complex increases and the free stream velocity is reached closer to the surface, resulting in a decreased δ .

The distances between the leading and trailing edges of these S. subterminalis-EP complexes were short and insufficient for a LBL to fully develop. When flow is deflected around a small structure, such as a S. subterminalis leaf, the flow curves behind the structure before the countervailing inertial and viscous forces can produce flow parallel to the surface. Rather than a LBL, there is a layer of water where flow streamlines do not cross and the increase in flow rate with distance from the surface asymptotically approaches the free-stream velocity. This layer is the hydrodynamic boundary layer (HBL). It is related to the diffusive boundary layer (DBL) in the same way as the LBL because lateral transport, across streamlines, must also be via molecular diffusion.

When average $\delta = \delta_{pred}$, epiphytic periphyton was absent and the S. subterminalis leaves were oriented approximately parallel to the bulk flow direction (Table 7). When average $\delta < \delta_{pred}$, periphyton was

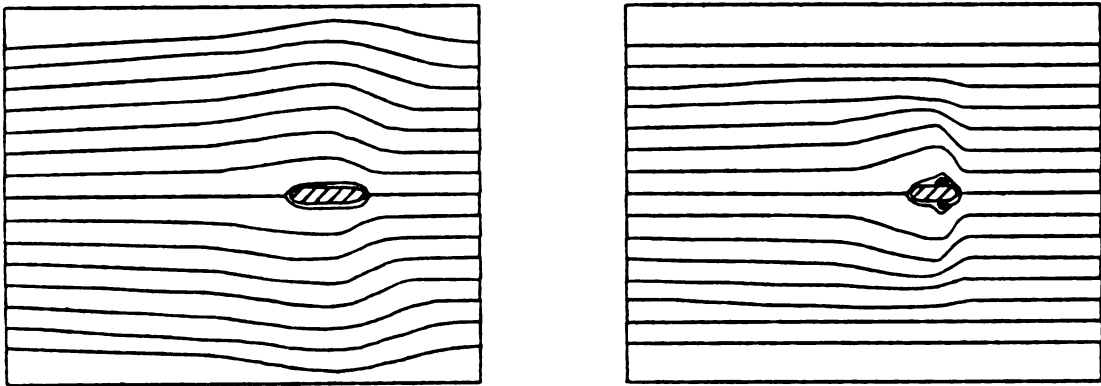


Figure 16. Conceptual illustration of right to left flow streamlines around small submersed plant leaf with and without epiphytic periphyton, right and left panels respectively.

present and/or leaf orientation was at an obtuse angle to bulk flow. When periphyton was absent, the S. subterminalis behaved as a flat plate oriented parallel to bulk flow direction. In the latter cases, the S. subterminalis-epiphytic periphyton complex width (projected perpendicular to flow), length (parallel to flow), and flow rate in combination determine the location of the inflection point and thickness of the δ . The effective width of the projected surface was a function of the periphyton biomass and leaf orientation, and the volume of displaced flow around the M-EP complex was a function of M-EP area projected perpendicular to flow multiplied by the bulk flow rate. Therefore, microscale flow pattern and thickness of the HBL surrounding the M-EP complex was dependent on shape, the ratio of width to length and location between leading and trailing edges of the perpendicular projection, and orientation to bulk flow direction. This is illustrated by comparing panels A and B of Figure 16 where the macrophyte leaf is oriented parallel to flow in both panels but is colonized with periphyton in panel B.

Epiphytic periphyton composition and structure ("type" = species composition and physical structure) are important parameters influencing the HBL thickness. Filamentous algae would tend to slow flow within the HBL and increase its thickness as a result of drag on the filament surfaces projecting above the periphyton canopy. Non-filamentous periphyton with a more closed canopy would increase the projected area of the complex without the decrease in flow rate caused by drag on the filaments. Longer algal filaments tend to orient with bulk flow and increase the effective length of the complex also contributing to a thicker HBL.

Previous estimates of non-turbulent boundary layer thickness have been far too small, $\approx 10 \mu\text{m}$ (Raven 1970, Smith and Walker 1980, Koch 1990). The hydrodynamic boundary layer (HBL) thickness for the S. subterminalis-epiphytic periphyton complex was on the order of 10^2 - $10^3 \mu\text{m}$ (Table 7). Diffusive resistance across the water column/M-EP

interface is much more significant than previously realized.

In this study, the largest δ measured was 2.46 mm. This was for a small but epiphyte free leaf at 0.16 cm s^{-1} . This flow rate is on the higher end of what was commonly found within beds; and therefore, is on the smaller end of the range of δ that occur for submersed plants in nature. The density of leaves in the dense 2-m S. subterminalis bed in Lawrence Lake was $0.5 \text{ leaves cm}^{-2}$ of sediment and the average distance between leaves was $\approx 18 \text{ mm}$. When a leaf was oriented with its flat surface parallel to flow, the thickness of δ was approximately inversely proportional to flow rate as predicted by the boundary layer equation. Therefore, δ for the lower end of flow rates found in this study ($\approx 0.04 \text{ cm s}^{-1}$) would be on the order of half the average distance between S. subterminalis leaves (9 mm). The water displaced around a S. subterminalis leaf will be limited to a distance, on average, of 9 mm from the surface as flow is constrained by flow around an adjacent leaf. The presents of periphyton and orientation of the leaf can reduce δ , and as a result, it would be rare that conditions be such that δ would be limited by the spatial distribution of S. subterminalis. However, when leaves of macrophytes with highly dissected leaves, such as Myriophyllum or Utricularia species, are oriented so that flow passes between the leaflets (this is most of the time), the δ will be limited by the spacing between those leaflets.

Diffusion is an integrative process driven by a concentration gradient toward a uniform concentration. The hydrodynamic boundary layer is related to the DBL through its affect on the water column rate of supply/sink of gases or dissolved substances. The supply/sink of gases or dissolved substances is maximal at the perimeter of the HBL because flow rate is greater and turbulent eddies occur. The relationship between HBL and DBL is not only dependent on the hydrodynamic characteristics of the M-EP complex (flow rate, viscosity, size (including projections) and orientation) but also on the rate of consumption/production of gases or dissolved substances within the

complex. If consumption/production rates are very high, the DBL may extend beyond the HBL. Conversely, if consumption/production rates are low, the DBL may not extend as far from the M-EP surface as the HBL. A diagnostic of the importance of hydrodynamics in diffusive transport is the shape of the DBL. As hydrodynamics increase in importance, the DBL more closely matches the HBL, rather than the shape the DBL would have if only diffusion were important. The shape of the DBL is affected by the shape of the M-EP complex even without flow. Jørgensen and Des Marais (1990) found that increased surface area, a result of increased microtopographic complexity of the benthic mat, resulted in an increased diffusive flux across the water column/mat interface. In addition, Carlton and Paerl (1989) found that oxygen tension surrounding filaments of Aphanizomenon flos-aquae (L.) Ralfs were regulated by the extension and contraction of algal aggregates. Upon elongation, the photosynthetically produced oxygen concentration decreased as a result of greater exposed surface area.

M-EP complex orientation to flow and shape, the size of projecting structures, are important parameters determining δ and, therefore, the diffusive path length across the water column/M-EP interface. My observations suggest that the leaves of lake littoral submersed macrophytes are randomly oriented with respect to flow direction, even though a predominance in flow direction may exist. There is no indication that macrophyte orientation is optimized to decrease the DBL. The type of epiphytic periphyton, however, can greatly affect the HBL and, consequently, the DBL as described above. Non-filamentous periphyton would tend to reduce the DBL, and filamentous periphyton would tend to increase the DBL.

Lower water temperatures result in higher viscosity and increased HBL thickness, which coincides with the high epiphyte biomass at the end of the macrophyte growing season. While the increased HBL decreases uptake from the water column, it also decreases loss of nutrients during senescence from the M-EP complex to the water column.

SUMMARY

The mean flow rate within the submersed littoral macrophyte beds was 0.07 cm s^{-1} and individual experiment means ranged from 0.03 cm s^{-1} to 0.46 cm s^{-1} . Water flows external to the beds were dissipated within the plant stand in less than 10-15 cm from the outer bed boundary even under severe conditions. Factors, such as submersed macrophyte bed depth and dominant species, had little affect on the variance of within-bed flow rates. Flow instability or separation associated with submersed macrophyte surfaces was only found at very high flow rates, or localized on the surface of the broad-leaved *P. praelongus* at moderate to fast within-bed flow rates.

There was insufficient distance for a laminar flow boundary layer (LBL) to develop over the narrow *S. subterminalis* leaves. However, the functional equivalent of the LBL, from the perspective of diffusive transport across the water column/M-EP interface, the hydrodynamic boundary layer (HBL), was found to form a layer much thicker than had been previously recognized, on the order of $10^3 \mu\text{m}$. Shape, the ratio of the length of projections from the M-EP surface perpendicular to flow to the length of the M-EP complex in the direction of flow, was important in determining the thickness of the HBL. Non-filamentous epiphytic periphyton had the effect of decreasing the HBL.

The low within-bed flow rates found in this study, indicate that flow separation associated with submersed macrophyte surfaces within beds is highly unlikely. When separation does occur, it is only during events with high winds and only at the very perimeter of the bed. The timing of high wind events further decreases the probability of flow separation associated with submersed plants within beds. These high wind events occur most frequently in seasons when the water temperature

is low, which offsets the higher flow rate because of the increased viscosity of water at lower temperatures.

Erosion of epiphytic periphyton from the surface of small-leaved macrophytes does not occur within beds but only on the perimeter during rare, very high wind events. Erosion from the surface of broad-leaved macrophytes within beds would also be rare. However, erosion from these leaf surfaces would occur more frequently at the perimeter of beds than for small-leaved plants. Additionally, broad-leaved plants colonizing open sites and not in beds, would experience erosion of periphyton from their leaf surfaces much more frequently. Because the plants are not within a bed, flow rates will be higher, and wind events of lower magnitude will result in erosion of epiphytic periphyton.

The results of this study support the hypothesis that submersed macrophytes and their epiphytic periphyton have a mutualistic relationship (Wetzel 1990), at least under oligo- and mesotrophic conditions. In low or moderately productive environments, rooted macrophyte productivity is governed in large part by sediment nitrogen and phosphorus concentrations. Epiphytic periphyton has the capacity to remove dissolved nutrients from the water column and to retain the captured nutrients within their biomass. The retention of nutrients is enhanced through the rapid cycling of nutrients as a result of the juxtaposition of the organisms within the layer (Wetzel 1990). Epiphytic periphyton greatly affects both the hydrodynamic and diffusive boundary layers (DBL), and the effect is dependent on the type (species composition and physical structure) of periphyton community. A non-filamentous complex has the effect of greatly decreasing the HBL causing a decrease in the DBL. In contrast, the large exposed surface area of a filament-dominated complex would increase the HBL as a result of the additional drag on the exposed surfaces. The larger HBL and greater diffusive resistance would offset the tendency toward increased nutrient uptake from the water column as a result of the greater exposed surface area.

I hypothesize the mechanism underlying the mutualism between the submersed macrophytes and their epiphytic periphyton to be as follows. Nutrients are taken up from the water column and retained within the M-EP complex during the growing season. While the boundary layer represents a barrier to the uptake of nutrients from the water column it also acts as a barrier to the diffusive loss of nutrients out of the complex. The juxtaposition of organisms within the M-EP complex ensures a rapid cycling and retention of nutrients within the layer maintaining a steep effective concentration gradient across the water column/M-EP interface. In most submersed macrophytes, nutrients are translocated to over-wintering structures, such as turions and rhizomes toward the end of the growing season (Sculthorpe 1967). Of the nutrients that are released from the macrophytes during senescence, many are retained within the complex. Increased filamentous algae and fungi at the end of the growing season coupled with increased viscosity, caused by decreased water temperature, combine to increase the HBL and resistance to diffusion of nutrients out of the M-EP complex. Further, the low within-bed flow rates ensure that upon senescence and collapse of the macrophytes, few nutrients are transported out of the community but are delivered to the sediments within the confines of the macrophyte bed. The increased fertility of the sediments enhances the growth of the macrophytes of the bed in the following season. Moeller et al. (1988) have demonstrated this synergistic mechanism in the retention of sedimentary phosphorus by Najas flexilis (Willd.) Rostk. and Schmidt and its epiphytic periphyton.

The decline in abundance of submersed macrophytes has been associated with increased eutrophication and increased epiphytic periphyton loading on macrophytes (e.g. Phillips et al. 1978). Filamentous algae often are an important feature of periphyton under nutrient enriched conditions. Under eutrophic conditions, dissolved inorganic carbon (DIC) may become limiting. While all nutrients are recycled within the M-EP complex, the pool of cycling DIC is very small

because a large proportion of carbon is incorporated into structural material. Under these conditions, filamentous algae are favored because the filaments protruding into the HBL tend to increase the HBL, decrease the supply of DIC from the water column and, at the same time, the filaments provide the algae access to higher concentrations of DIC. The fertile sediments, low concentration of DIC within the M-EP complex and superior shading characteristics of filamentous algae (Losee 1983, Losee and Wetzel 1983) combine to break down the mutualistic association of submersed macrophyte and epiphytic periphyton under progressive eutrophication.

APPENDIX

APPENDIX

Five-channel, Warm-bead Thermistor Flowmeter

Circuit (Figure 17)

The five-channel, warm-bead thermistor flowmeter used in this study was based on the design of Vogel (1981) with modifications that increased spatial and temporal resolution of littoral flow rate measurements. The principle of operation for the flowmeter was as follows. An electrical current passing through a thermistor bead heated the bead to an equilibrium temperature that was a function of the electrical power applied and the heat dissipation characteristics of the surrounding medium. Cooling by forced convection was a strong function of flow rate. The sensing thermistor formed one arm of a Wheatstone bridge circuit with a temperature-compensating thermistor in the parallel arm of the circuit. Because the resistance of the compensating thermistor was 40-times that of the sensing thermistor, virtually all electrical current passed through the sensing thermistor arm of the bridge, thus, heating the sensing thermistor but not the compensating thermistor. In this isothermal circuit, where the sensing thermistor was maintained at a set temperature above ambient, the electrical power required to maintain the temperature offset of the thermistor was a function of flow rate. The electrical potential across the arms of the bridge circuit drove the transistor as part of a feedback-loop, which regulated electrical current flow through the bridge circuit and maintained the offset temperature of the sensing thermistor above ambient. This electrical potential was also amplified in an isolation circuit to provide a voltage output proportional to flow rate.

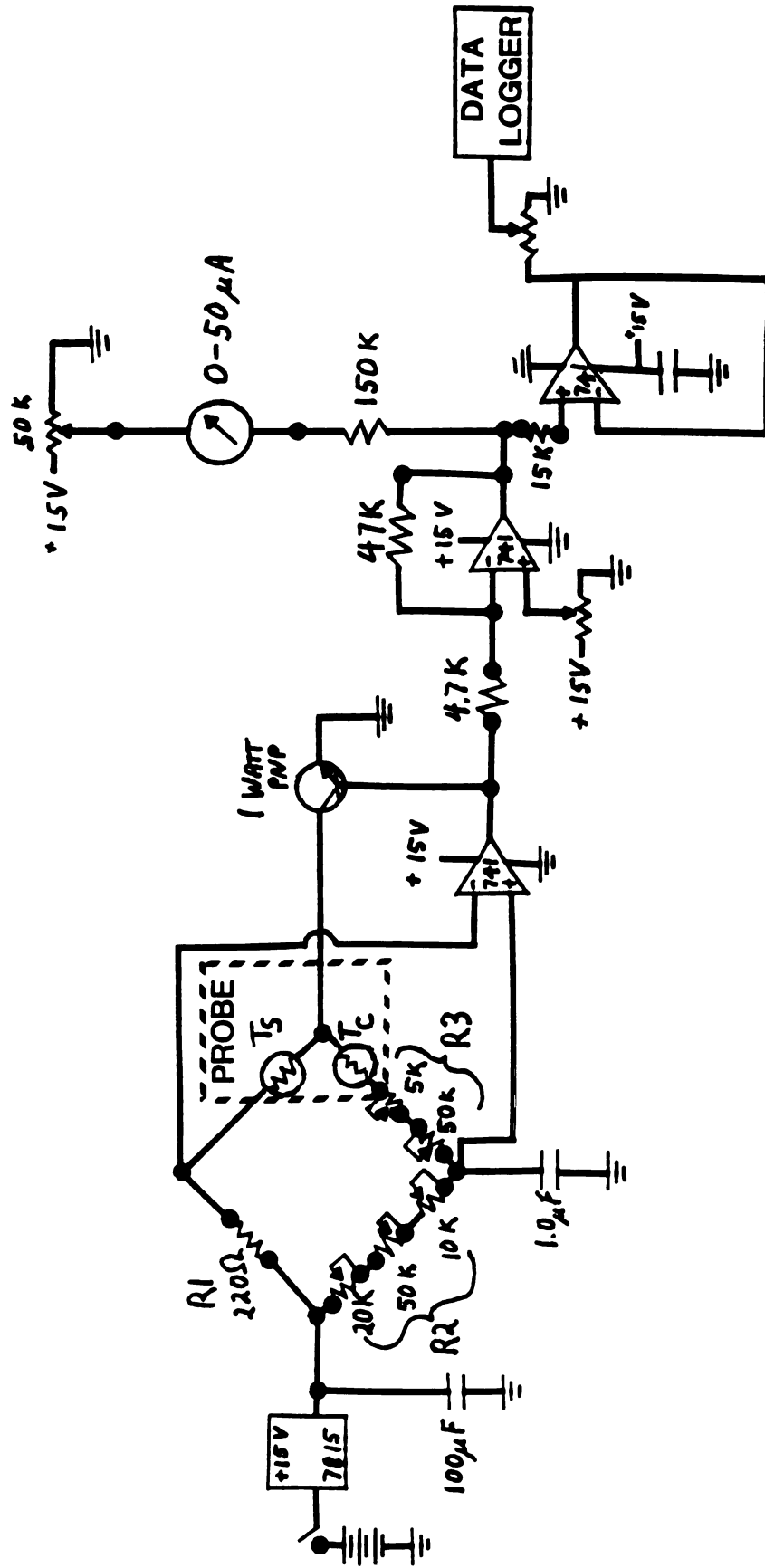


Figure 17. Flowmeter circuit schematic.

Probe

The sensing and temperature-compensating thermistor half of the bridge circuit was assembled into a compact probe connected with the second half of the bridge and meter amplification circuits via a multi-conductor submersible cable. A small sensing thermistor, 0.4-mm diameter (Thermometrics, Inc., BR16KA251M, nominal resistance 250 Ohms), was used to improve spatial and temporal resolution by decreasing probe size and thermal inertia. The temperature-compensating thermistor was Thermometrics, Inc., Model BR32KB103M, nominal resistance 10K Ohms. Forstner and Rützler (1969) and Riedl and Machan (1972) discuss hot-bead thermistor flow measurement theory; the latter paper provides guidelines for choosing thermistors and bridge-balancing resistors.

Adjusting temperature range and zero

Before calibrating a flow probe and companion circuit, the bridge circuitry was balanced to provide a stable voltage output for a range of water temperatures, and the voltage output nulled for zero flow. The meter maintained a stable reading over a range of 8° to 10° C. The probe, with flow-sensing and temperature-compensating thermistors, was placed in a still water chamber at the upper bound of the temperature range, and the offset voltage across the bridge adjusted to 4.5 V. The offset voltage across the bridge set the level of self heating of the sensing thermistor above ambient temperature. The probe was alternately placed in the low and high temperature still water chambers and the equilibrium offset voltage in the low temperature chamber noted. The probe was returned to the high temperature chamber and the bridge circuit adjusted and balanced until the offset voltage was stable at the temperature extremes. Because of the sensitivity of the circuit, great care was taken to ensure no water movement occurred in the still water chamber. Observation with a dissecting microscope of "still" water baths revealed that water movement occurred virtually all of the time unless special precautions were taken. The still water chamber was

placed into a well-mixed water bath. It was necessary to guard against development of temperature stratification in the water baths as this quickly induced convection currents. To dampen convection currents during the temperature ranging and zeroing procedure, polyester wool was placed in the bottom of the 16 x 150 mm culture tube used as the still water chamber. Loose fibers assisted in dampening any water movement within the tube. Caution was taken to ensure the sensing thermistor was not too near the tube sidewall or fibers as these materials have heat transfer coefficients different from water and would cause an error in adjusting the zero flow point. In addition, there was a tendency for the tap water in the still water chamber to degas at atmospheric pressure with the sensing thermistor bead providing a nucleation site for bubble formation. Therefore, the tap water was degassed by boiling while under a vacuum before use.

Calibration

To calibrate the meter, a known, adjustable, and hydrodynamically smooth flow was required. A nozzle was developed which provided a non-turbulent, "plug" flow: i.e., within the nozzle outlet tube, flow rate was constant across the entire cross-section. For calibration, the sensing thermistor portion of a probe was positioned at the base of the outlet tube where flow entered from the nozzle body. Flow rate in the outlet was determined by measuring the volume output per time divided by the outlet cross-sectional area.

The nozzle consisted of a 4.44 cm I.D. clear acrylic tube 12.5 cm long with a 1.27 cm I.D. acrylic inlet nipple and 2.54 cm I.D. outlet port made of a 4.5 cm long acrylic tube. On the inlet side of the nozzle, a polyester wool plug held behind a Nitex screen was used to equalize pressure across the entire diameter of the nozzle body. Two additional Nitex screens were placed at intervals in the nozzle with the last screen 5.5 cm from the outlet orifice to smooth flow within the nozzle. The Nitex screens had a 20 μ m pore size. The intersection of

the nozzle sidewall and outlet end cap was beveled to smoothly direct flow into the outlet port. The nozzle was positioned vertically with the outlet directed upward. A small reservoir with an overflow outlet was mounted over the nozzle outlet port. Water flowing through the nozzle filled the reservoir and flowed out the overflow outlet where flow, as volume per time, was measured. A dye injected into the flow stream was used to determine whether flow was non-turbulent and uniform across the nozzle outlet port. To achieve non-turbulent plug flow at the outlet orifice required some trial-and-error manipulation of the end cap bevel and screen placement. The probe tip was placed in the outlet port within 1 to 3 mm of the nozzle body. This ensured that flow was uniform across the entire cross-section at the point where flow rate was measured.

Two methods were used to provide adjustable flow rates. A centrifugal pump was used to provide fast flow rates, employing a gate valve or hose clamp to regulate flow. As flow rates were decreased by restricting flow, unsteady flow occurred. Therefore, for slow flow rates, a system was developed where a differential head was used to regulate flow. A reservoir was constructed with an overflow outlet which maintained a constant water level at the overflow height. The reservoir height could be raised or lowered to adjust the head differential with the nozzle, thus regulating flow rate. Flowing water was conducted via flexible tubing (1.27 mm I.D.) from the reservoir or centrifugal pump to the nozzle.

MacIntyre (1986) showed self heating to interfere with flow rate measurements for rates less than 0.3 cm s^{-1} for a similar warm-bead thermistor flowmeter. However, self heating was not evident for this meter even at very slow flow rates. The panels of Figure 18 show the measured calibration curves and predicted flow rates versus flowmeter millivolts output for each probe and circuit. A natural logarithm transformation of flow rates provided a very good conversion equation. The predicted flow versus millivolts values agree closely with the

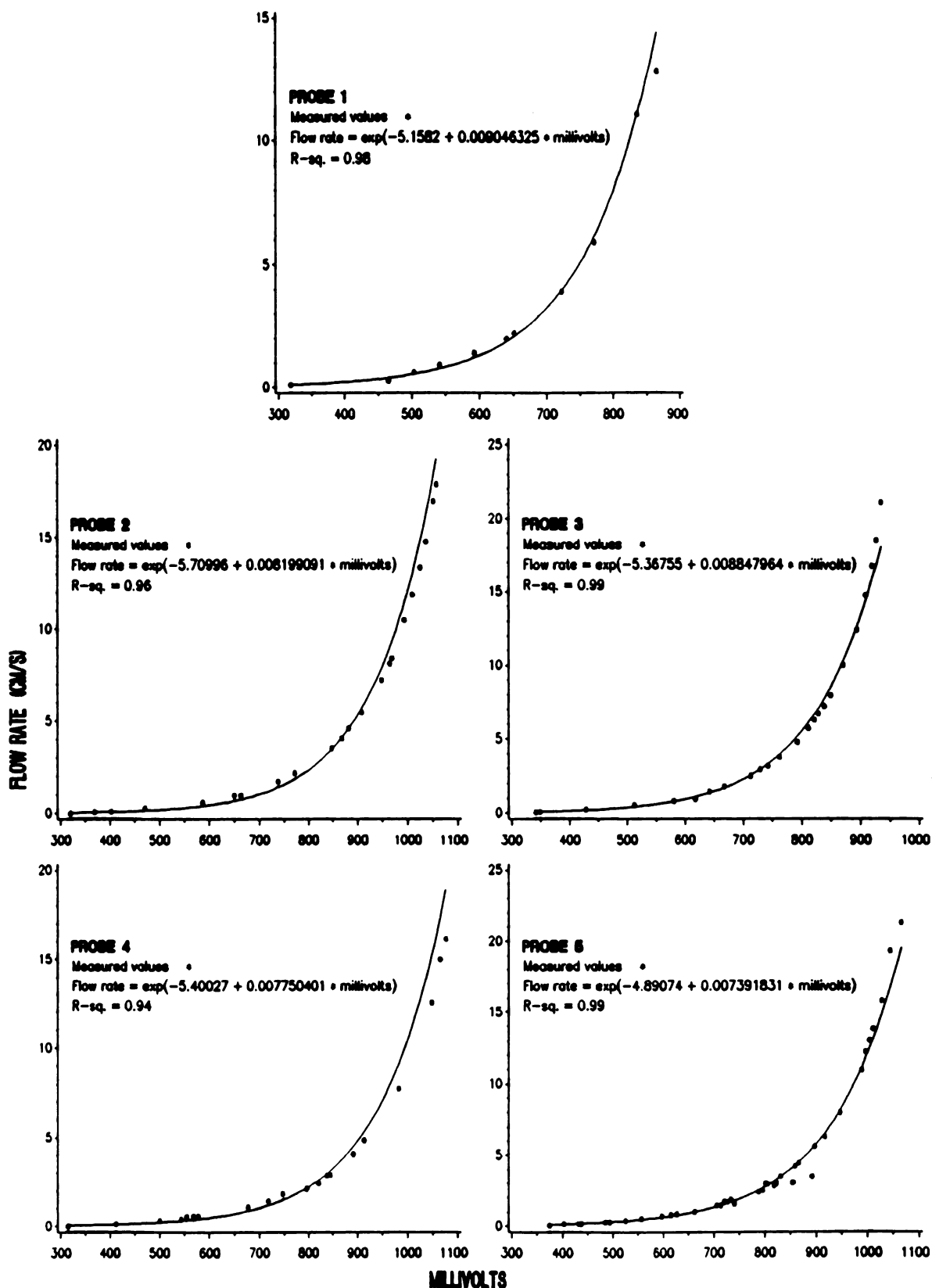


Figure 18. Measured calibration curve and predicted flow rate versus flowmeter millivolts output for each probe and paired circuit.

measured values even at very low flow rates.

Meter stability was tested by recording the voltage output of the meter while the probe was placed in the still water chamber or in the calibration nozzle. In both cases, the meter output was smooth unless turbulence occurred in the calibration nozzle. When flow in the calibration nozzle was turbulent, rapid fluctuations in flow rate were recorded as a result of the turbulent eddies passing the sensing thermistor.

LIST OF REFERENCES

LIST OF REFERENCES

- Ackerman, J.D. 1986. Mechanistic implications for pollination in the marine angiosperm Zostera marina. Aquatic Botany 24:343-353.
- Barth, H. 1957. Aufnahme und Abgabe von CO₂ und O₂ bei submersen Wasserpflanzen. Gewässer Abwässer 4(17/18):18-81.
- Burkholder, J.M. and R.G. Wetzel. 1989. Microbial colonization on natural and artificial macrophytes in a phosphorus-limited, hardwater lake. Journal of Phycology 25:55-65.
- Burkholder, J.M. and R.G. Wetzel. 1990. Epiphytic microalgae on natural substrata in a hardwater lake: Seasonal dynamics of community structure, biomass and ATP content. Archive Hydrobiologia/Supplement 83:1-56.
- Carlton, R.G. and H.W. Paerl. 1989. Oxygen-induced changes in morphology of aggregates of Aphanizomenon flos-aquae (Cyanophyceae): implications for nitrogen fixation potentials. Journal of Phycology 25:326-333.
- Crank, J. 1975. The Mathematics of Diffusion. Oxford Press, New York.
- Fonseca, M.S., J.S. Fisher, J.C. Zieman, and G.W. Thayer. 1982. Influence of the seagrass, Zostera marina L., on current flow. Estuarine, Coastal and Shelf Science 15:351-364.
- Forstner, H. and K. Rützler. 1969. Two temperature-compensated thermistor current meters for use in marine ecology. Journal of Marine Research 27:263-271.
- Gamma Design Software. 1991. Geostatistics for the Agronomic and Biological Sciences. Version 1.1.
- Gavis, J. 1976. Munk and Riley revisited: nutrient diffusion transport and rates of phytoplankton growth. Journal of Marine Research 34:161-179.
- Happel, J. and H. Brenner. 1973. Low Reynolds Number Hydrodynamics. Noordhoff International Publishing, Leyden.
- Jørgensen, B.B. and D.J. Des Marais. 1990. The diffusive boundary layer of sediments: Oxygen microgradients over a microbial mat. Limnology and Oceanography 35:1343-1355.
- Gundersen, J.K. and B.B. Jørgensen. 1990. Microstructure of diffusive boundary layers and the oxygen uptake of the sea floor. Nature 345:604-607.
- Koch, A.L. 1990. Diffusion: the crucial process in many aspects of the biology of bacteria. Advances in Microbial Ecology 11:37-70.
- Leyton, L. 1975. Fluid Behavior In Biological Systems. Claredon Press, Oxford.

- Losee, R.F. 1983. Characterization of Selective Light Attenuation by Periphyton. M.S. Thesis, Michigan State University, East Lansing, Michigan.
- Losee, R.F. and R.G. Wetzel. 1983. Selective light attenuation by the periphyton complex. In: Periphyton of Freshwater Ecosystems, R.G. Wetzel (ed.). Dr. W. Junk Publishers, Boston.
- Losee, R.F. and R.G. Wetzel. 1988. Water movement within submersed littoral vegetation. Verhandlungen Internationale Vereinigung Limnologie 23:62-66.
- Machata-Wenninger, C. and G.A. Janauer. 1991. The measurement of current velocities in macrophyte beds. Aquatic Botany 39:221-230.
- MacIntyre, S. 1986. A flow-measuring system for use in small lakes. Limnology and Oceanography 31:900-906.
- Madsen, T.V. and M. Søndergaard. 1983. The effects of current velocity on the photosynthesis of Callitriche stagnalis Scop. Aquatic Botany 15:187-193.
- Madsen, T.V. and E. Warncke. 1983. Velocities of currents around and within submerged aquatic vegetation. Archive Hydrobiologia 97:389-394.
- Moeller, R.E., J.M. Burkholder, and R.G. Wetzel. 1988. Significance of sedimentary phosphorus to a rooted submersed macrophyte (Najas flexilis (Willd.) Rostk. and Schmidt) and its algal epiphytes. Aquatic Botany 32:261-281.
- Moss, B. 1972a. Studies on Gull Lake, Michigan I. Seasonal and depth distribution of phytoplankton. Freshwater Biology 2:289-307.
- Moss, B. 1972b. Studies on Gull Lake, Michigan II. Eutrophication-evidence and prognosis. Freshwater Biology 2:308-320.
- Munk, W.H. and G.A. Riley. 1952. Absorption of nutrients by aquatic plants. Journal of Marine Research 11:215-240.
- Olson, J.S. 1958. Rates of succession and soil changes on southern Lake Michigan dunes. Botanical Gazette 19:125-170.
- Phillips, G.L., D. Eminson, and B. Moss. 1978. A mechanism to account for macrophyte decline in progressively eutrophicated freshwaters. Aquatic Botany 4:103-126.
- Raven, J.A. 1970. Exogenous inorganic carbon sources in plant photosynthesis. Biological Reviews 44:167-221.
- Rich, P.H., R.G. Wetzel, and N.V. Thuy. 1971. Distribution, production and role of aquatic macrophytes in a southern Michigan marl lake. Freshwater Biology 1:3-21.
- Riedl, R.J. and R. Machan. 1972. Hydrodynamic patterns in lotic intertidal sands and their bioclimatological implications. Marine Biology 13:179-209.
- Riber, H.H. and R.G. Wetzel. 1987. Boundary-layer and internal diffusion effects on phosphorus fluxes in lake periphyton. Limnology and Oceanography 32:1181-1194.

- Robertson, G.P. 1987. Geostatistics in ecology: Interpolating with known variance. *Ecology* 68:744-748.
- SAS Institute. 1988. SAS User's Guide: Statistics. SAS Institute, Cary, North Carolina, USA.
- Schumacher, G.J. and L.A. Whitford. 1965. Respiration and P^{32} uptake in various species of freshwater algae as affected by a current. *Journal of Phycology* 1:78-80.
- Sculthorpe, C.D. 1967. *Biology of Aquatic Vascular Plants*. St. martins Press, New York.
- Silvester, N.R. and M.A. Sleight. 1985. The forces on microorganisms at surfaces in flowing water. *Freshwater Biology* 15:433-448.
- Smith, F.A. and N.A. Walker. 1980. Photosynthesis by aquatic plants: effects of unstirred layers in relation to assimilation of CO_2 and HCO_3^- and to carbon isotopic discrimination. *New Phytologist* 86:245-259.
- Van Dyke, M. 1982. *An Album of Fluid Motion*. The Prabolic Press, Stanford.
- Vogel, S. 1981. *Life In Moving Fluids. The Physical Biology of Flow*. Princeton University Press.
- Webster, R. 1985. Quantitative spatial analysis of soil in fields. *Advances in Soil Science* 3:1-70.
- Westlake, D.F. 1967. Some effects of low-velocity currents on the metabolism of aquatic macrophytes. *Journal of Experimental Botany* 18:187-205.
- Wetzel, R.G. 1990. Land-water interfaces: metabolic and limnological regulators. *Verhandlungen Internationale Vereinigung Limnologie* 24:6-24.
- Wheeler, W.N. 1980. Effect of boundary layer transport on the fixation of carbon by the giant kelp Macrocystis pyrifera. *Marine Biology* 56:103-110.
- Whitford, L.A. and G.J. Schumacher. 1961. Effect of current on mineral uptake and respiration by a fresh-water alga. *Limnology and Oceanography* 6:423-425.